*

CUSPS AND CORES IN GALAXIES:PROBLEMS AND SOLUTIONS

Antonino Del Popolo

Dep. of Physics and Astronomy, Catania University

October, UFES, Vitoria

*

Outline

- Lecture 1:

  -The problem of "cusps" in CDM dark matter haloes
  -Density profiles in dwarf, spiral, elliptical galaxies, and in clusters

- Lecture 2,3:

  -Proposed solutions (old ideas):
  -Problems in observations
  -Problems in simulations

  Proposed solutions ("new ideas"):
  -Different DM particles
  -Modified gravity
  -Heating of the Cusp: Supernovae feedback
  -Heating of the Cusp: dynamical friction of baryonic clumps on DM

- Lecture 4?:

  -The other small scale problems of the LCDM
  -Unified baryonic solution

- Concluding Remarks

*

LECTURE1:

Dark matter distribution in galaxies and clusters

The ΛCDM Model

- **ΛCDM:** model parameterization of the Big Bang cosmological model in which the universe contains a cosmological constant (**Λ**), and cold dark matter.
- Frequently referred to as the **standard model** of Big Bang cosmology or **Cosmic Concordance Model** , since it is the simplest model that provides a reasonably good match to the following observations:
- the existence and structure of the **cosmic microwave background**
- the large scale structure in the distribution of galaxies
- the **abundances of hydrogen (including deuterium), helium, and lithium**
- the accelerating **expansion of the universe** observed in the light from distant galaxies and **supernovae**

*

Structure formation

WMAP 7

$\Omega_{Tot}=1.080^{+0.093}_{-0.071}$

$\Omega_{\Lambda}=0.734\pm0.029$

$\Omega_{m}=0.222\pm0.026$

$\Omega_{b}=0.0449\pm0.0028$

$H_0=71.0\pm2.5$ km/s/Mpc

$t_0=13.75\pm0.13$ Gyr

Planck

$\Omega_b h^2$	$0.022\,30 \pm 0.000\,14$	4.9%
$\Omega_c h^2$	0.1188 ± 0.0010	26.8%(68.3%)
t_0	$13.799 \pm 0.021 \times 10^9$ years	
n_s	0.9667 ± 0.0040	

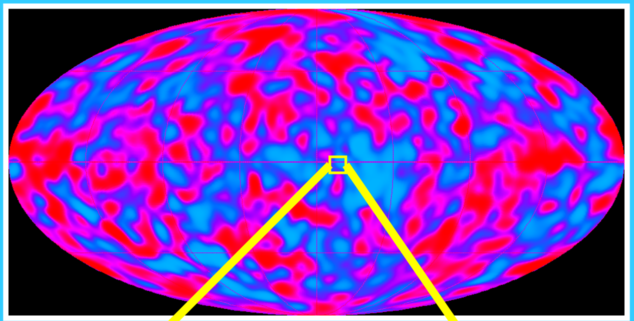

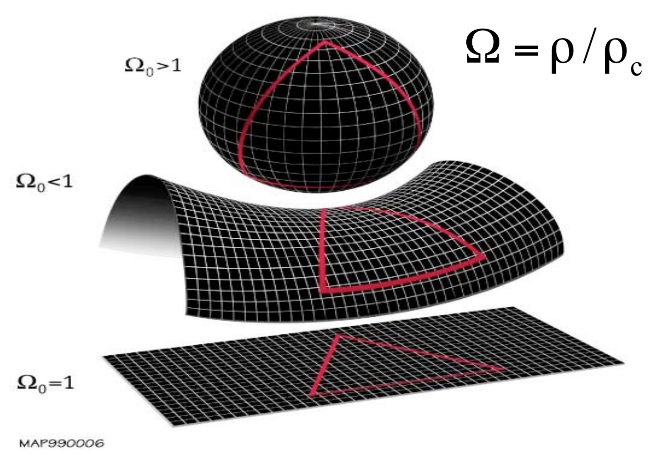

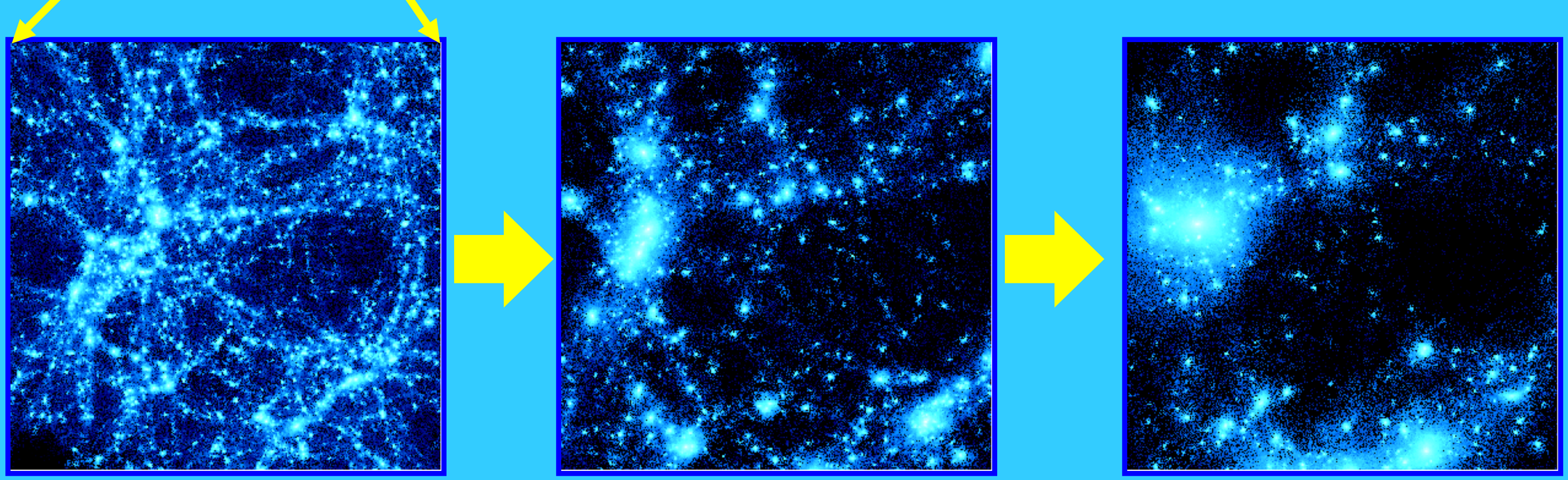

Small Scale Challenges for CDM

➔ Despite successes of ΛCDM on large and intermediate scales, serious issues remain on smaller, galactic and sub-galactic, scales. In particular:

1. Missing satellite problem: High predicted number of small haloes

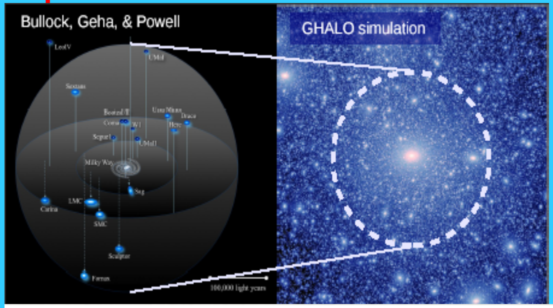

2. Too Big To Fail: Dissipationless ΛCDM simulations predict that the majority of the most massive subhaloes of the Milky Way are too dense to host any of its bright satellites

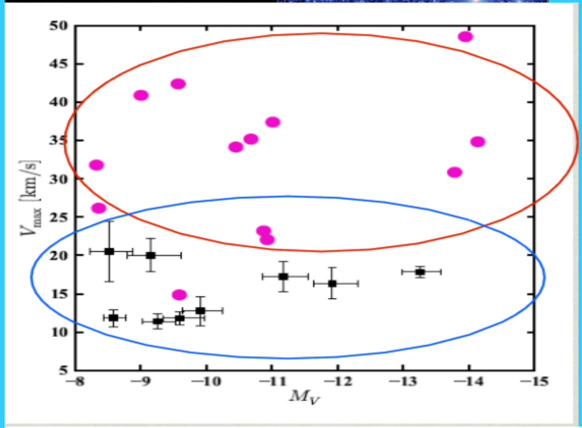

3. Angular momentum catastrophe: Low angular momentum of baryons, and consequent small radius of disks

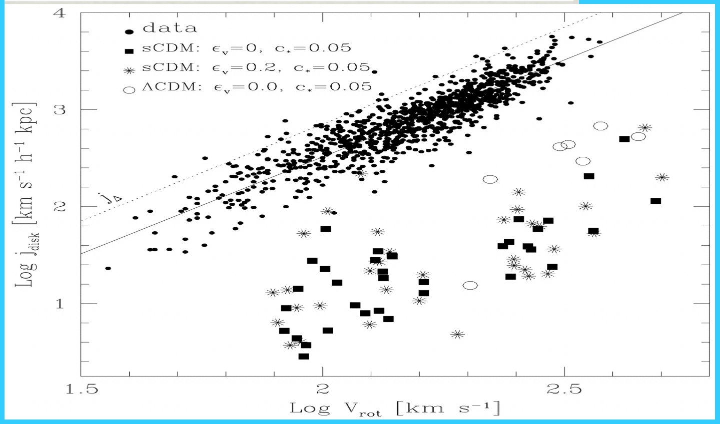

4. CUSP/CORE PROBLEM

- Cusp/Core Problem: **Dark matter cusps absent in galaxy centers, LSBs and dwarf Irr (CDM dominated)**

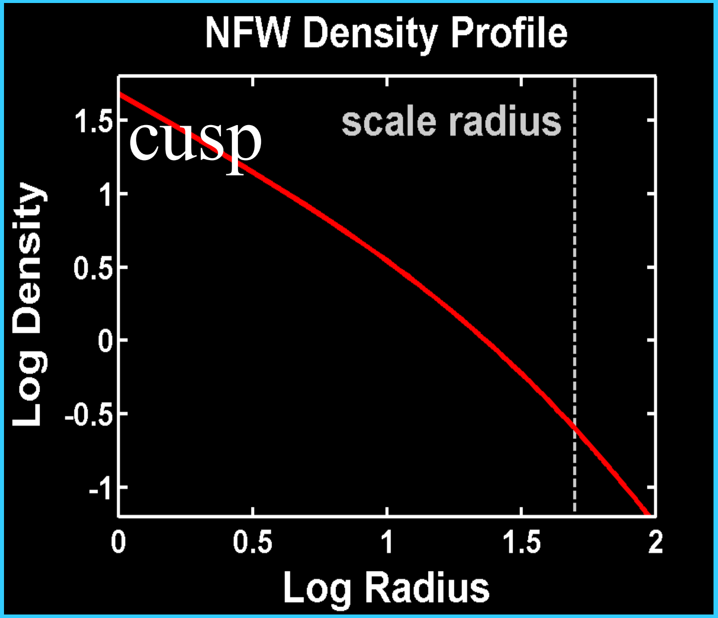

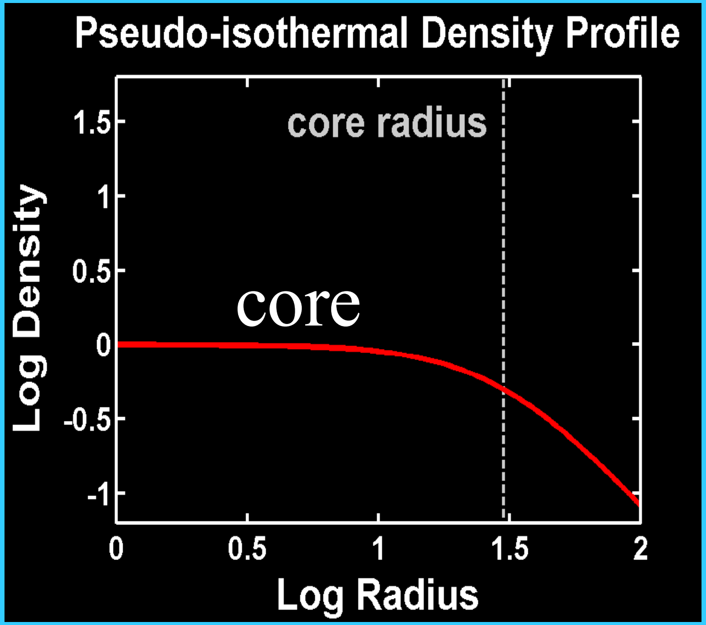

Flores & Primack 1994
Moore 1994
Swaters et al. (2003)
Diemand et al. (2004)
Simon et al. (2005)
De Blok et al. (2008)
Kuzio de Naray and Kaufmann (2011)

Parametrize density profile as $\rho(r) \propto r^{-\alpha}$
- Observations show $\alpha \sim 0$ (constant-density core)
- Simulations predict $\alpha \sim 1$ (central cusp)

*

Density profiles of haloes: a short story

Power law profiles:

1970: **Peebles** - N-body simulation (N=300).

1972: **Gunn & Gott** - dissipationless collapse of a spherical homogeneous perturbation in a expanding Friedmann universe.

1977: **Gott** - secondary infall model $\rho \propto r^{-9/4}$. Spherical inhomogeneous perturbation + shell crossing

1984, 1985: Fillmore & Goldreich; Bertschinger - self-similar solutions collapse scale-free spherical perturbation

1985: Hoffman & Shaham - Predicted that density profile around density peaks is $\rho \propto r^{-3(n+3)/(n+4)}$

1986: **Quinn, Salmon & Zurek** - N-body simulations (N$\sim$10000), confirmed $\rho \propto r^{-3(n+3)/(n+4)}$

1988: **Frenk, White, Davis & Efstathiou** - N-body simulations ($N=32^3$) - CDM flat rotation curve out to 100kpc

1990: **Hernquist** - Analytic model with a central cusp for elliptical galaxies - $\rho \propto r^{-1}(r+r_s)^{-3}$

Non power law profiles:

>1990: **Dubinski & Carlberg (1991), Lemson (1995), Cole & Lacey (1996), Navarro et al. (1995; 1996, 1997)(NFW)...**

\+ **Moore et al. (1998), Jing & Suto (2000), Klypin et al. (2001), Bullock et al. (2001), Power et al. (2003); Navarro et al. (2004), Stadel et al (2008), Springel et al. (2008), Navarro et al. 2010.**

*

Navarro, Frenk & White (1997)

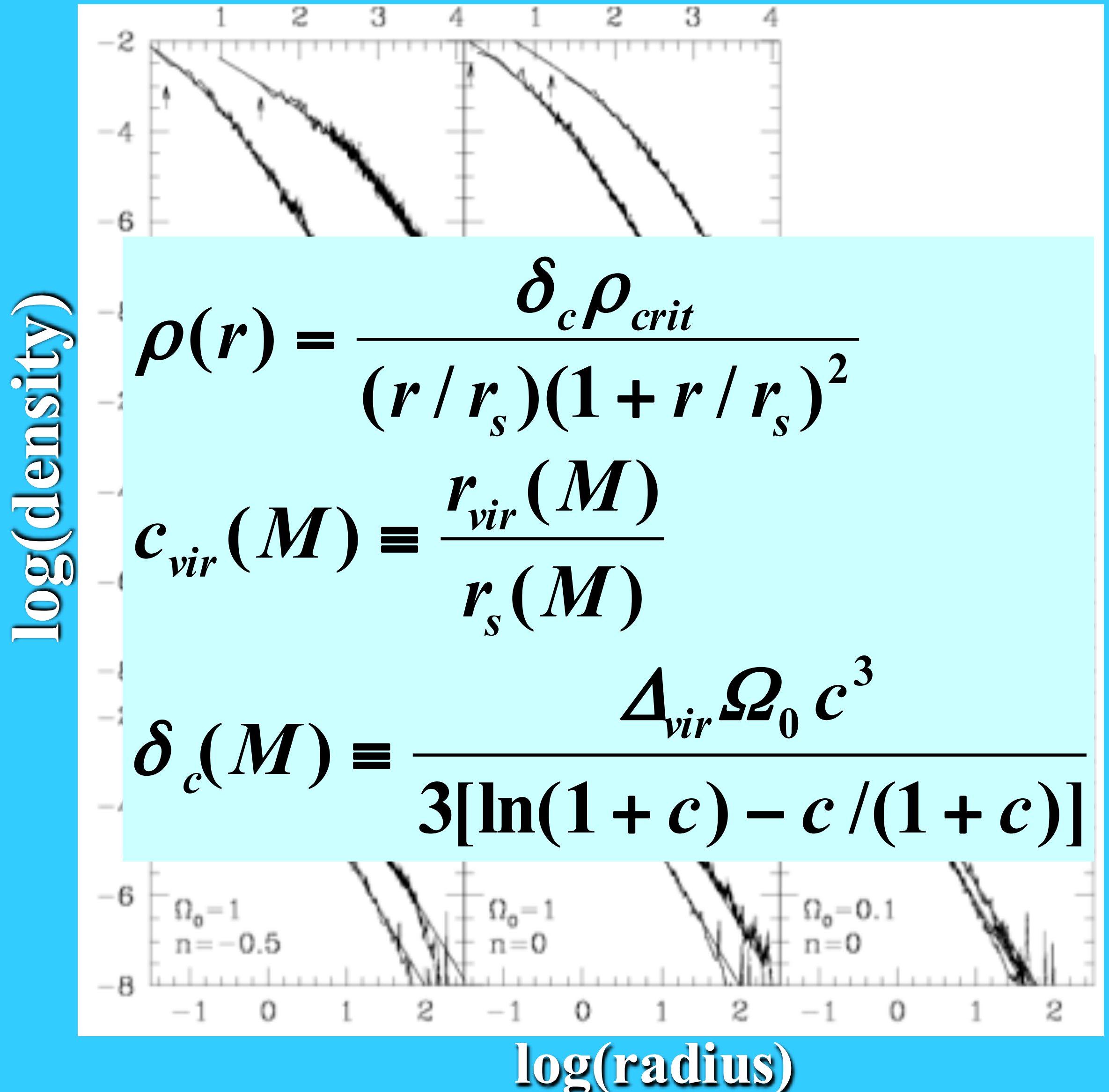

$$\rho(r) = \frac{\delta_c \rho_{crit}}{(r/r_s)(1+r/r_s)^2}$$

$$c_{vir}(M) \equiv \frac{r_{vir}(M)}{r_s(M)}$$

$$\delta_c(M) \equiv \frac{\Delta_{vir}\Omega_0\, c^3}{3[\ln(1+c) - c/(1+c)]}$$

- Asymptotic outer slope -3; inner -1
- Halo density profile is independent of cosmological initial conditions
- Scaled density profile of the most massive and least massive halos look very similar except at the core
- The less massive halo has higher density at the center possibly due to the fact that they form earlier, and density perturbations at earlier times of the universe are more concentrated

*

- Higher resolution simulations, which resolves more of the inner region of the halos, found steeper inner slopes (Moore et al. 1998,1999; Jing & Suto (2000) Fukushige & Makino 2001)

- Moore et al. 1998,1999 ; Fukushige & Makino 2001: steeper inner slope:

$$\rho \propto r^{-1.5}$$

- Jing & Suto (2000), Ricotti (2003): haloes profiles are not universal. In comoving coordinates, r, the profile is

$$\rho_{\rm dm} \propto \frac{1}{X^{\alpha}(1+X)^{3-\alpha}}$$

$$X = c_{\Delta} r / r_{\Delta} \text{ and } \alpha = (9+3n)/(5+n) \approx 1.3 + (M_{\rm dm,14}^{1/6} - 1)/(M_{\rm dm,14}^{1/6} + 1)$$

$$M_{\rm dm,14} = M_{\rm dm}/(3 \times 10^{14}\ {\rm M}_{\odot})$$

r_{Δ} virial radius

n effective spectral index

$$n_{\rm eff} = \left.\frac{{\rm d}\ln P(k)}{{\rm d}\ln k}\right|_{k=1/R_c}$$

From dwarfs o clusters for any z

*-

Jing & Suto (2000)

~ $5 \times 10^{12} M_{sun}$

~ $5 \times 10^{13} M_{sun}$

~ $3 \times 10^{14} M_{sun}$

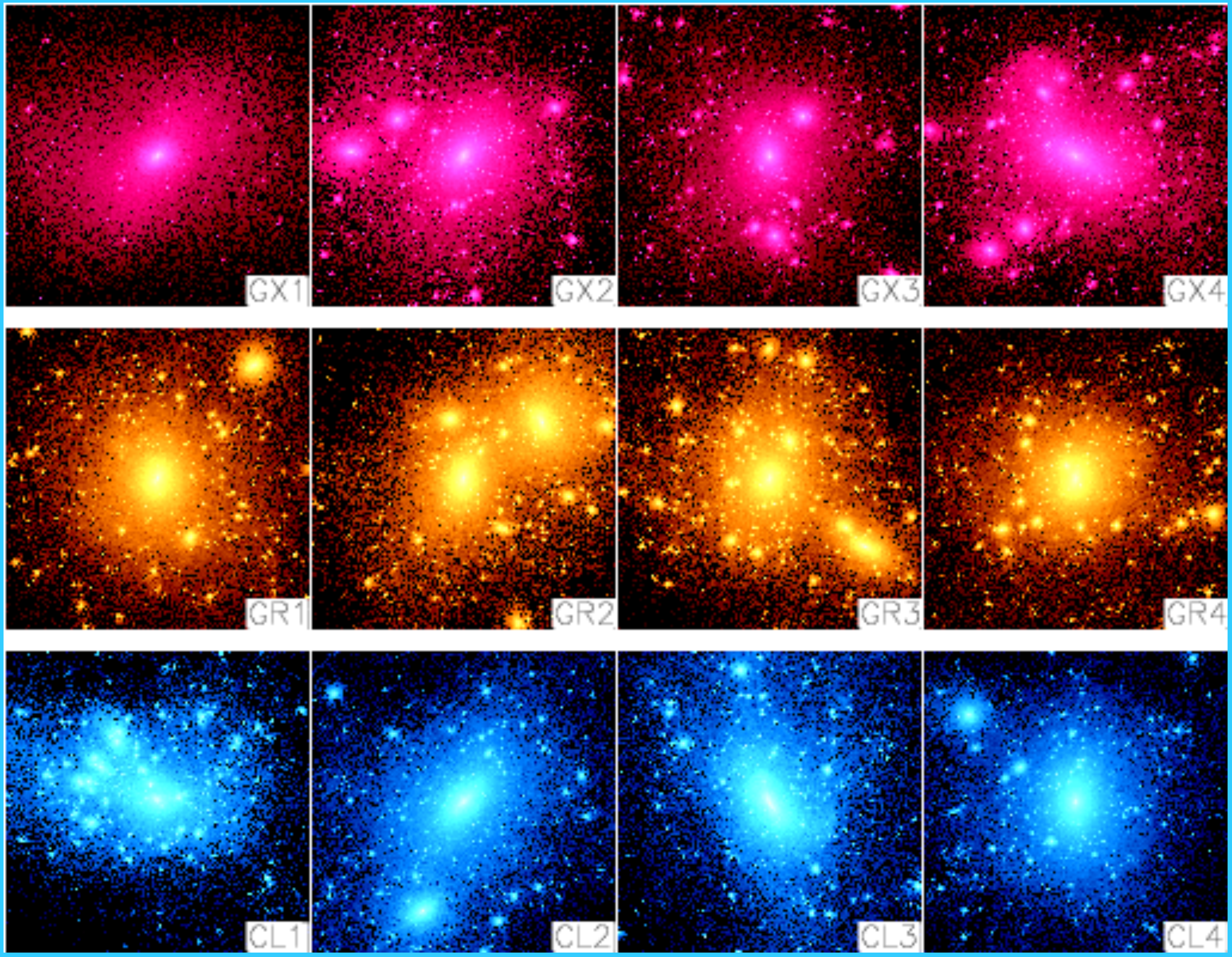

*-

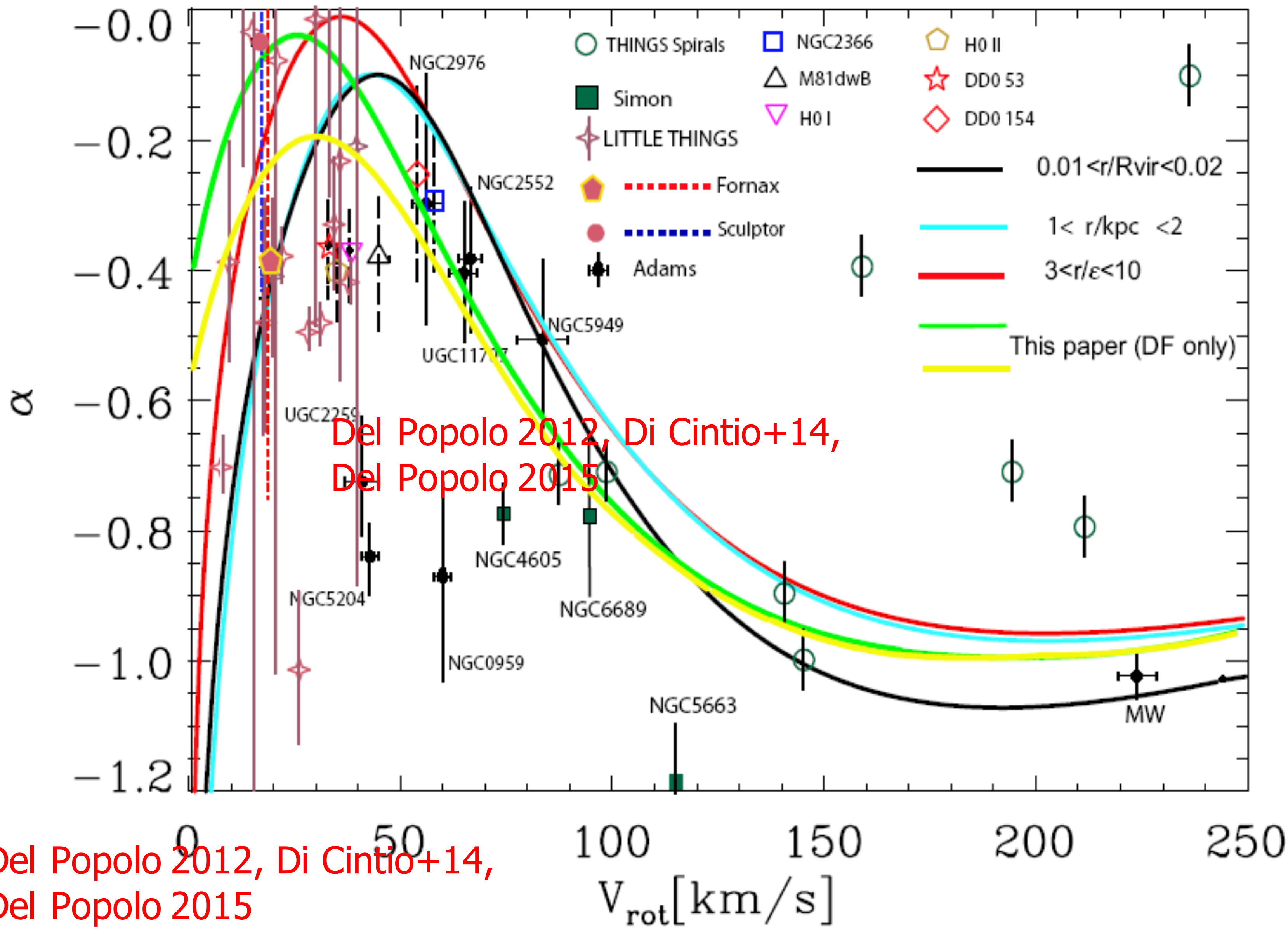

Del Popolo 2012, Di Cintio+14,
Del Popolo 2015

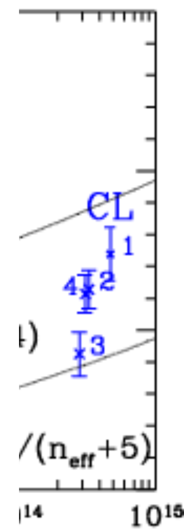

Del Popolo 2012, Di Cintio+14,
Del Popolo 2015

*-

Fukushige & Makino (1997)

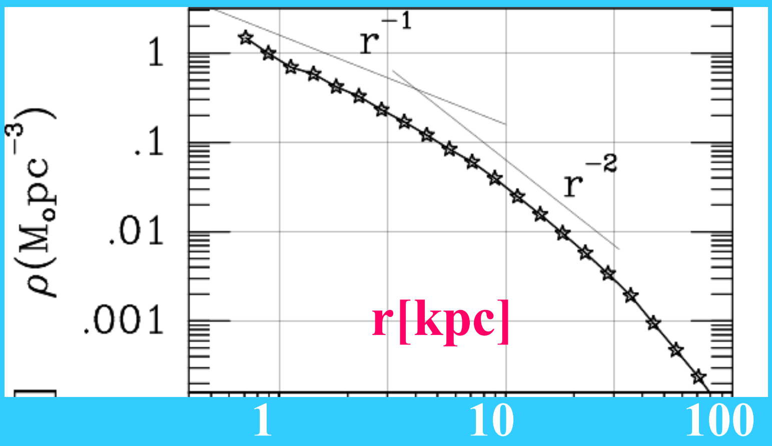

- inner slope in higher-resolution simulations is steeper (~ –1.5) than the NFW value (–1.0)

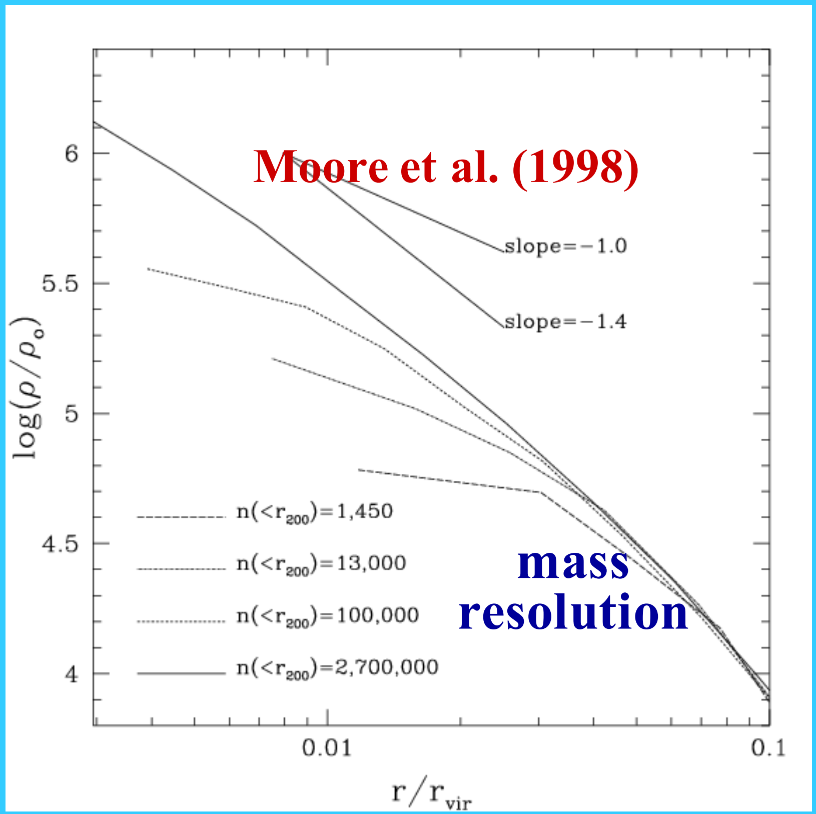

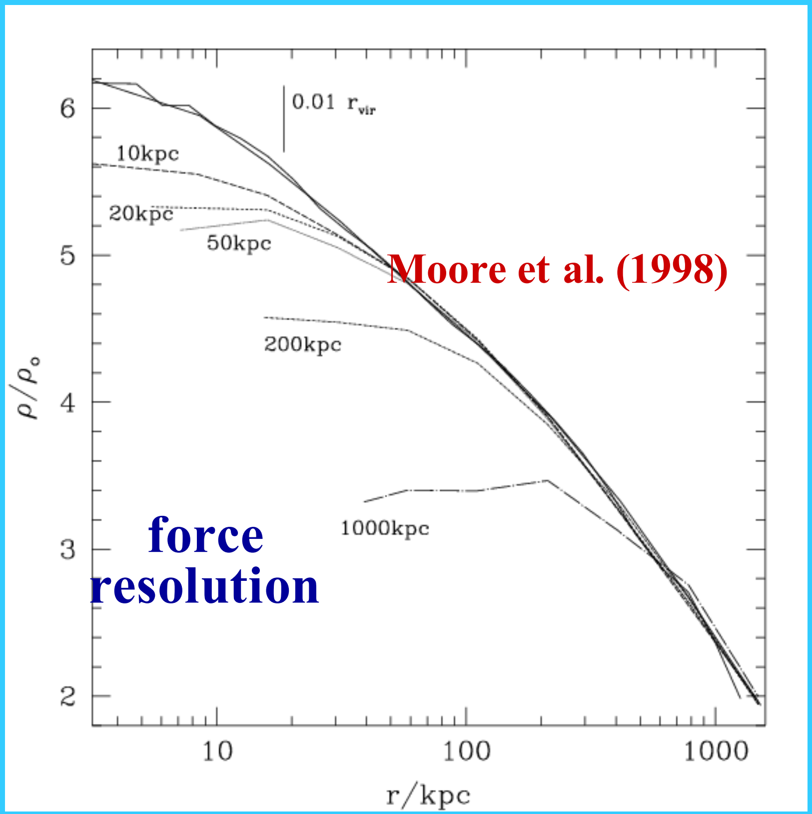

*-

New Models

- Navarro et al (2004, 2010) proposed a new analytic form:

$$\ln(\rho_\alpha/\rho_{-2}) = (-2/\alpha)[(r/r_{-2})^\alpha - 1]$$

Where r_{-2} is defined as the radius at which:

$$\beta = -d\log\rho/d\log r = 2$$

•The profile slope is now varying with radius to 0.5% of r_{200}

•Profile becomes shallower with r->0, No asymptote, slope at 120 pc, -0.8 (Stadel+09)

Slope mass depending:
(Ricotti 2003, Ricotti & Wilkinson 2004; Ricotti et al. 2007; Del Popolo 2009, 2010; Di Cintio et al. 2014)

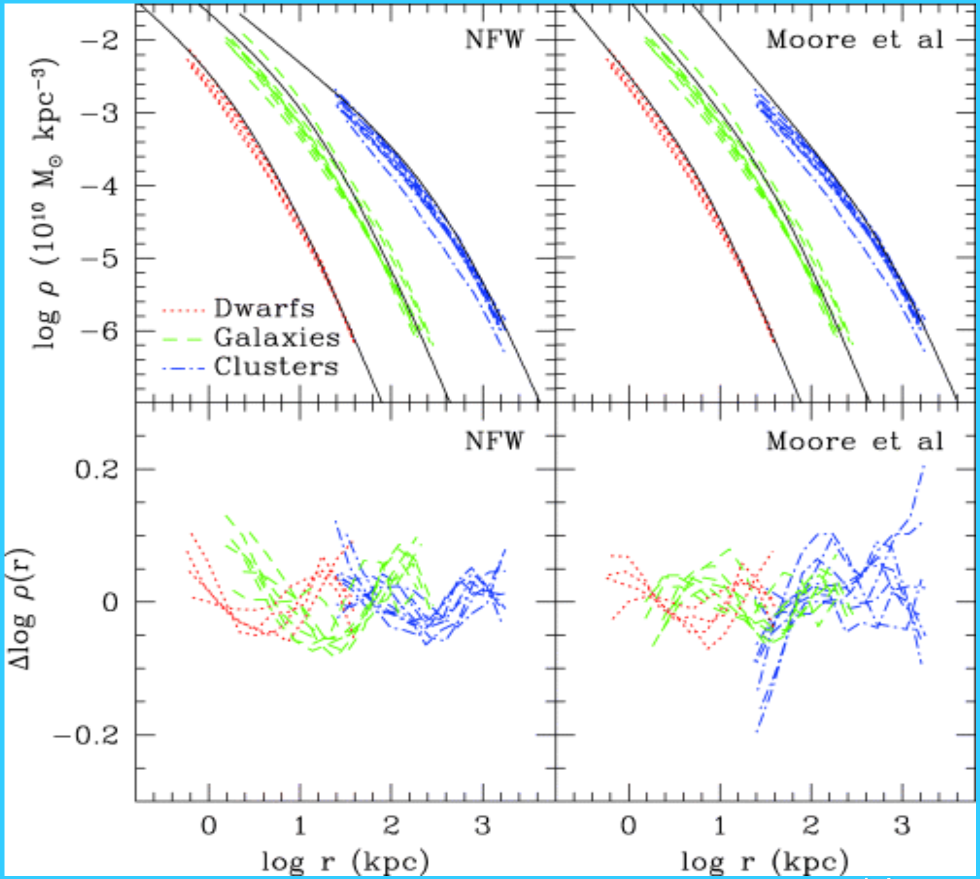

Stadel et al. (2008)
(mass resolution 1000
Solar masses. Slope
at 0.05% Rvir (120 pc) is -0.8)

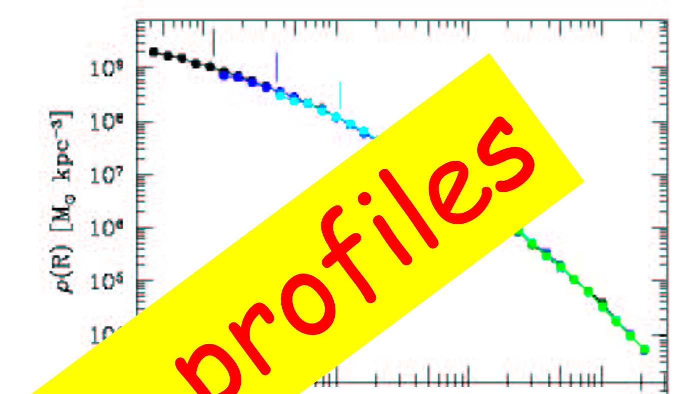

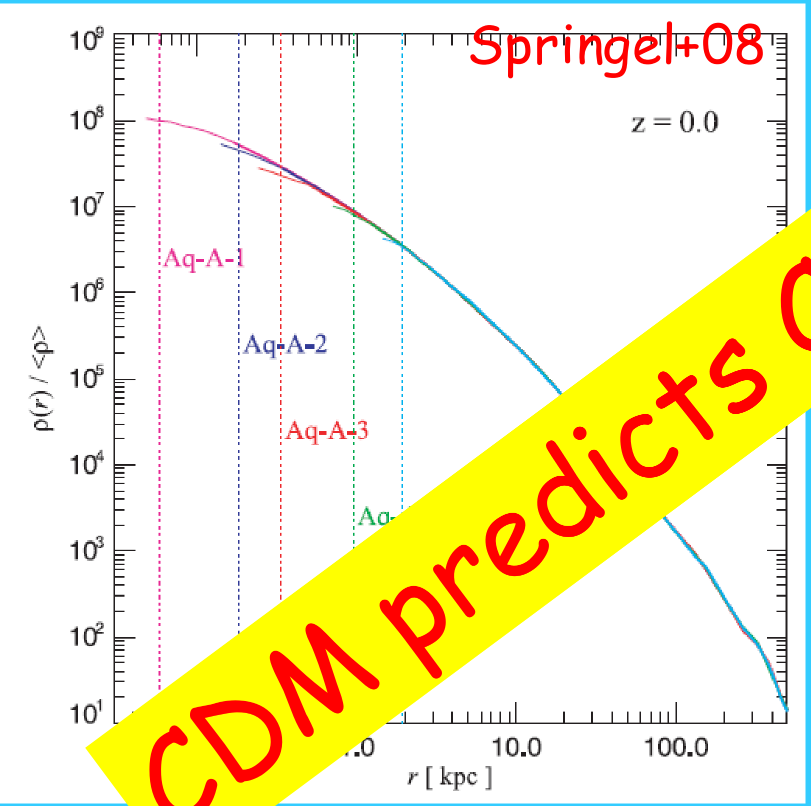

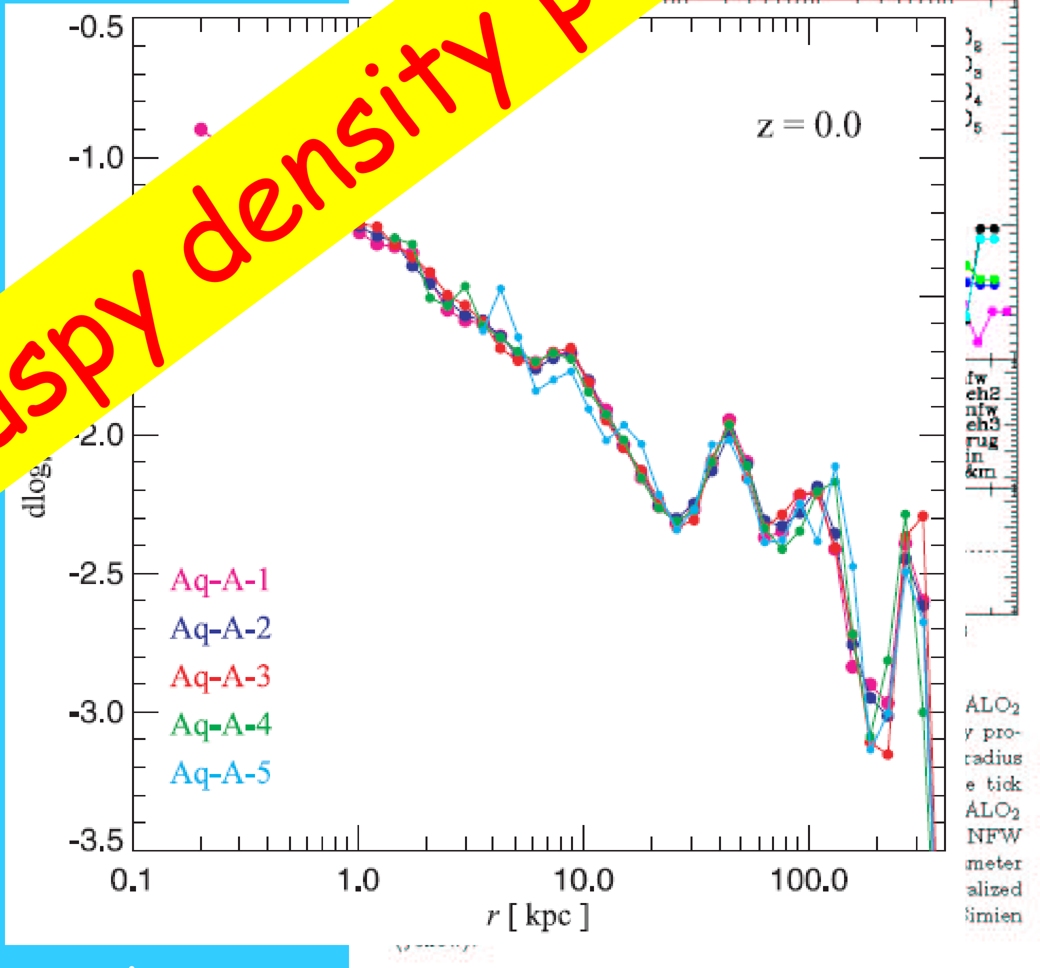

CDM predicts Cuspy density profiles

No asymptotic slope detected so far

SUMMARIZING

- Profiles of dark matter are not power laws
- Profiles of dark matter are cuspy in the central region (but α>-1 -> NFW not correct)
- The value of inner slope is debated (α_{min} ~-0.8)
- A large number of simulations predict that universal profiles of dark matter halos are universal (NFW or Einasto) (at least approximately; but see Jing & Suto 2000, Ricotti 2003; Ricotti & Wilkinson, 2004; Ricotti Pontzen & Viel 2007; Del Popolo 2010, Del Popolo 2011)

DENSITY PROFILES IN SPIRALS (ROTATION CURVES)

Stellar Disks

M33 - outer disk truncated, very smooth structure

NGC 300 - exponential disk goes for at least 10 scale-lengths

$$I(r) = I_0 e^{-r/R_D}$$

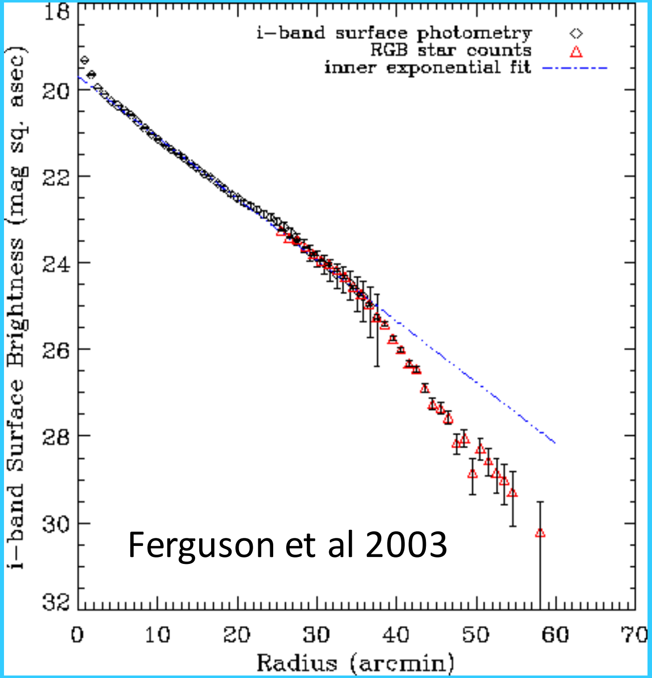

Ropt=3.2R$_D$

scale radius

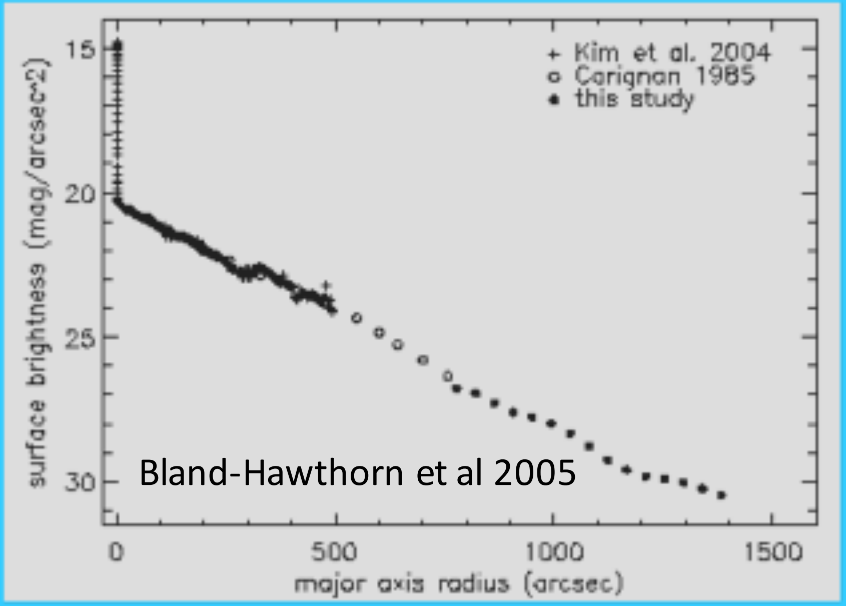

Gas surface densities

GAS DISTRIBUTION

HI

Flattish radial distribution

Deficiency in centre

CO and H_2

Roughly exponential

Negligible mass

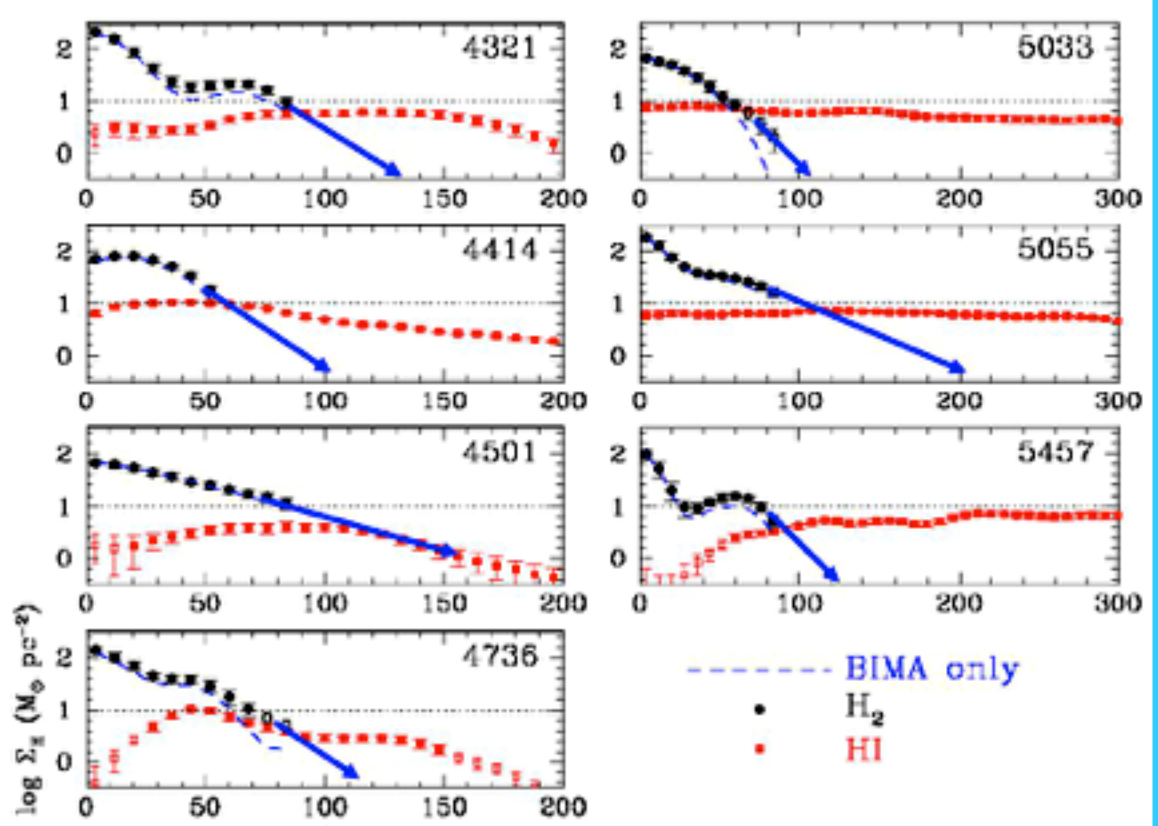

Wong & Blitz (2002)

Berkeley-Illinois-. Maryland Association (**BIMA**) Array with 30 GHz receivers.

Circular velocities from spectroscopy

- Optical emission lines (Hα, Na)

- Neutral hydrogen (HI)-carbon monoxide (CO)

HI -> 21 cm
CO -> mm -> range [e.g., 115.27 GHz for ^{12}CO (J = 1 -0) line, 230.5 GHz for J =(2 -1)

Tracer	angular resolution resolution	spectral
HI	7" … 30"	2 … 10 km s^{-1}
CO	1.5" … 8"	2 … 10 km s^{-1}
Hα, …	0.5" … 1.5"	10 … 30 km s^{-1}

ROTATION CURVES(RCs)

A RC is obtained calculating the rotational velocity of a tracer (e.g. stars, gas) along the length of a galaxy by measuring their Doppler shifts, and then plotting this quantity versus their respective distance away from the centers

Tracing the intensity-weighted velocities

$$V_{\rm int} = \int I(v) v dv / \int I(v) dv$$

I(v)= intensity profile at a given radius as a function of the radial velocity.

The rotation velocity is then given by

i= inclination angle

Vsys= systemic velocity of the galaxy.

$$V_{\rm rot} = (V_{\rm int} - V_{\rm sys}) / \sin\, i$$

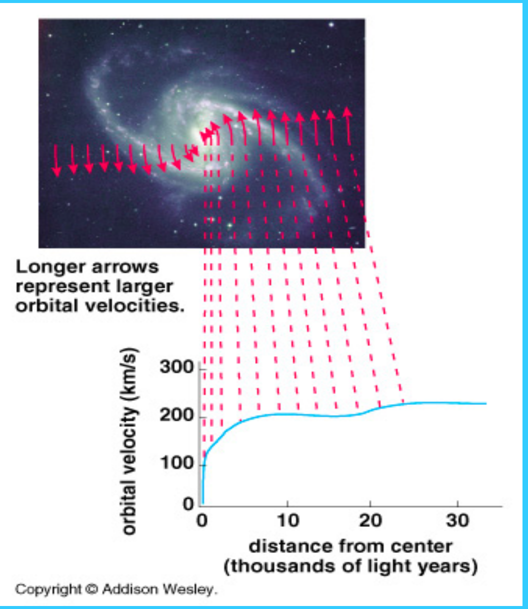

.

UGC2405

EXAMPLE OF HIGH QUALITY RC

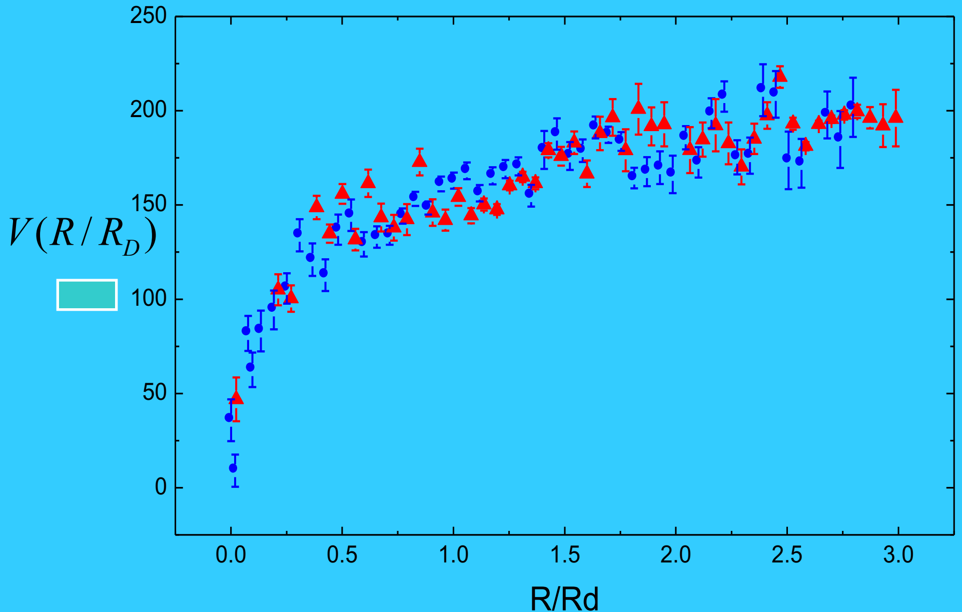

Optical resolution: 2", i.e. RD/30-RD/10

Radio Interferometers: 10"

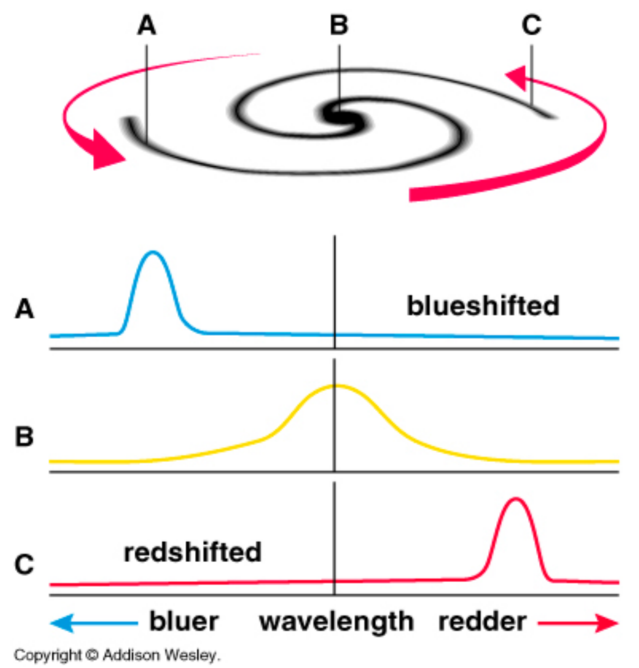

Rotation curve analysis

From data to mass models

observations $\rightarrow$ $V_{tot}^2 = V_{halo}^2 + V_{disk*}^2 + V_{HI}^2 + (V_b^2)$ $\leftarrow$ model

Model parameters

M_D, r_0, ρ_0

- V^2_{disk} **from I-band photometry** $V^2_{disk,*} = \dfrac{GM_D}{2R_D} x^2 B(\dfrac{x}{2})$ $\quad x = r/R_D$ $\quad B = I_0K_0 - I_1K_1$
- V^2_{HI} **from HI observations**
- V^2_{halo} **different choices for the DM halo density** $\leftarrow$ $\rho(r) = \dfrac{\rho_0}{(1+r/r_0)(1+(r/r_0)^2)}$

Dark halos with cusps (NFW, Einasto)

$$\rho(r)/\rho_{crit} \approx \delta\; r_s / r(1 + r/r_s)^2$$

$$V(R) = V_{200}\left[\frac{\ln(1+cx) - cx/(1+cx)}{x[\ln(1+c) - c/(1+c)]}\right]^{1/2}$$

$$\ln\; \rho(r)/\rho_{-2} = -2/\alpha\; [(r/r_{-2})^\alpha - 1]$$

Dark halos with constant density cores (Burkert)

$$\rho(r) = \frac{\rho_0}{(1+r/r_0)(1+(r/r_0)^2)}$$

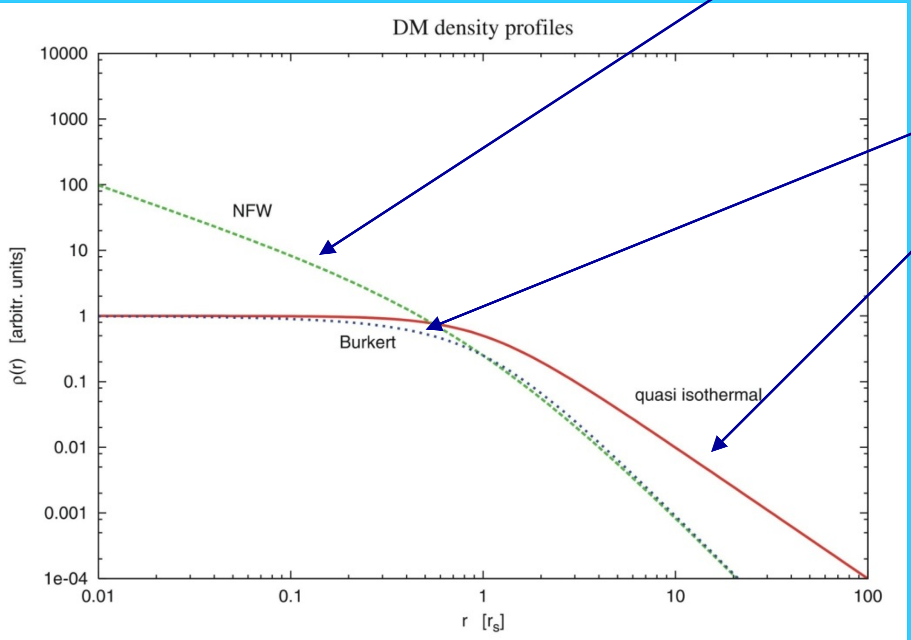

$$\rho_{ISO}(R) = \rho_0\left[1 + \left(\frac{R}{R_C}\right)^2\right]^{-1}$$

$$V(R) = \sqrt{4\pi G\rho_0 R_C^2\left[1 - \frac{R_C}{R}\arctan\left(\frac{R}{R_C}\right)\right]}$$

Model has three free parameters: disk mass, halo central density and core radius (halo length-scale)

Obtained by best fitting method.

*

Cusp/Core:Observational controversy: LSB rotation curves

- Flores & Primack 1994; Moore 1994: Flat rotation curves of the low surface brightness (LSB) galaxies -> halos are not going to be singular

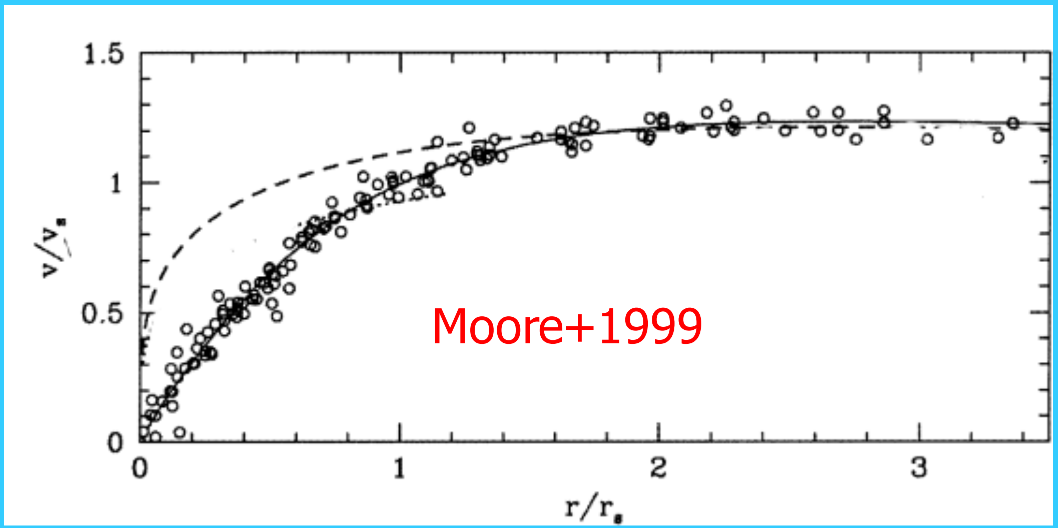

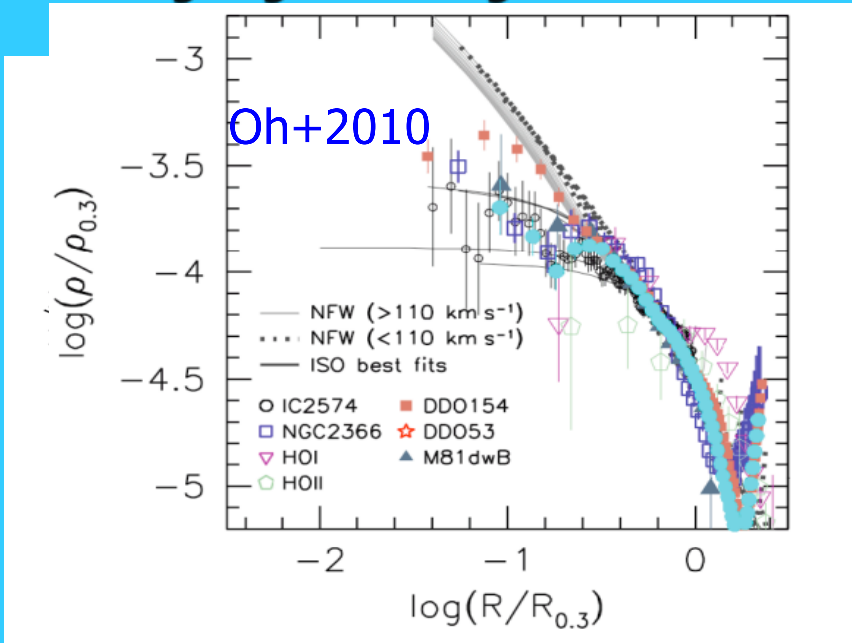

Other studies: Burkert 1995; de Blok & Bosma 2003, Gentile et al. 2008, Spano et al. 2008, de Blok et al. 2009, Oh et al. 2010; Kuzio de Naray & Kaufmann 2011, Oh et al. 2015 (LITTLE THINGS)

⇨ **Shape of density profile is shallower than that found in numerical simulations (e.g., 0.2 ± 0.2)**

*

Gentile et al. 2004, 2007

- **Rotational curves of spiral galaxies : stellar, + gas + dark matter**
- **Fitting the density with various models**
- **Constant density core models preferred**

Burkert: with a DM core

$\rho = \rho_s/(1+r/r_s)(1+(r/r_s)^2)$

NFW

$\rho = \rho_s/(r/r_s)(1+r/r_s)^2$

Moore

$\rho = \rho_s/(r/r_s)^{1.5}(1+(r/r_s)^{1.5})$

HI-scaling const. factor,

MOND without DM

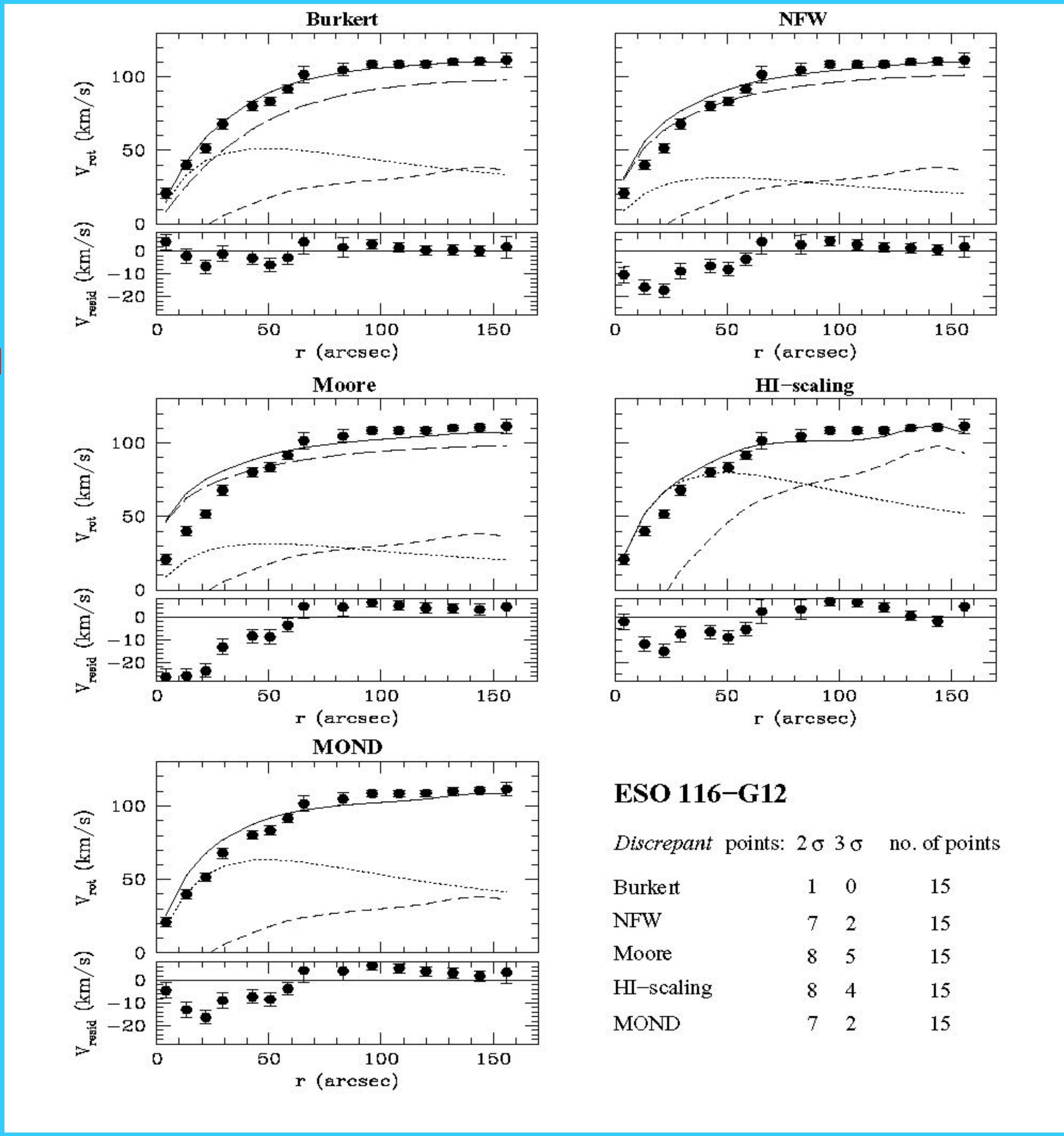

Mass models for the galaxy Eso 116-G12. Solid line: best fit, long-dashed line: DM halo; dotted: stellar; dashed: gaseous disc. 1kpc = 13.4 arcsec. Below: residuals: (V_{obs}-V_{model})

GALAXIES PROFILES COMPATIBLE WITH CORES?

de Blok et al. (2008):

•(high mass spirals) galaxies having $M_B < -19$ -> NFW profile or a PI profile;

• (low mass spirals) $M_B > -19$ -> PI model

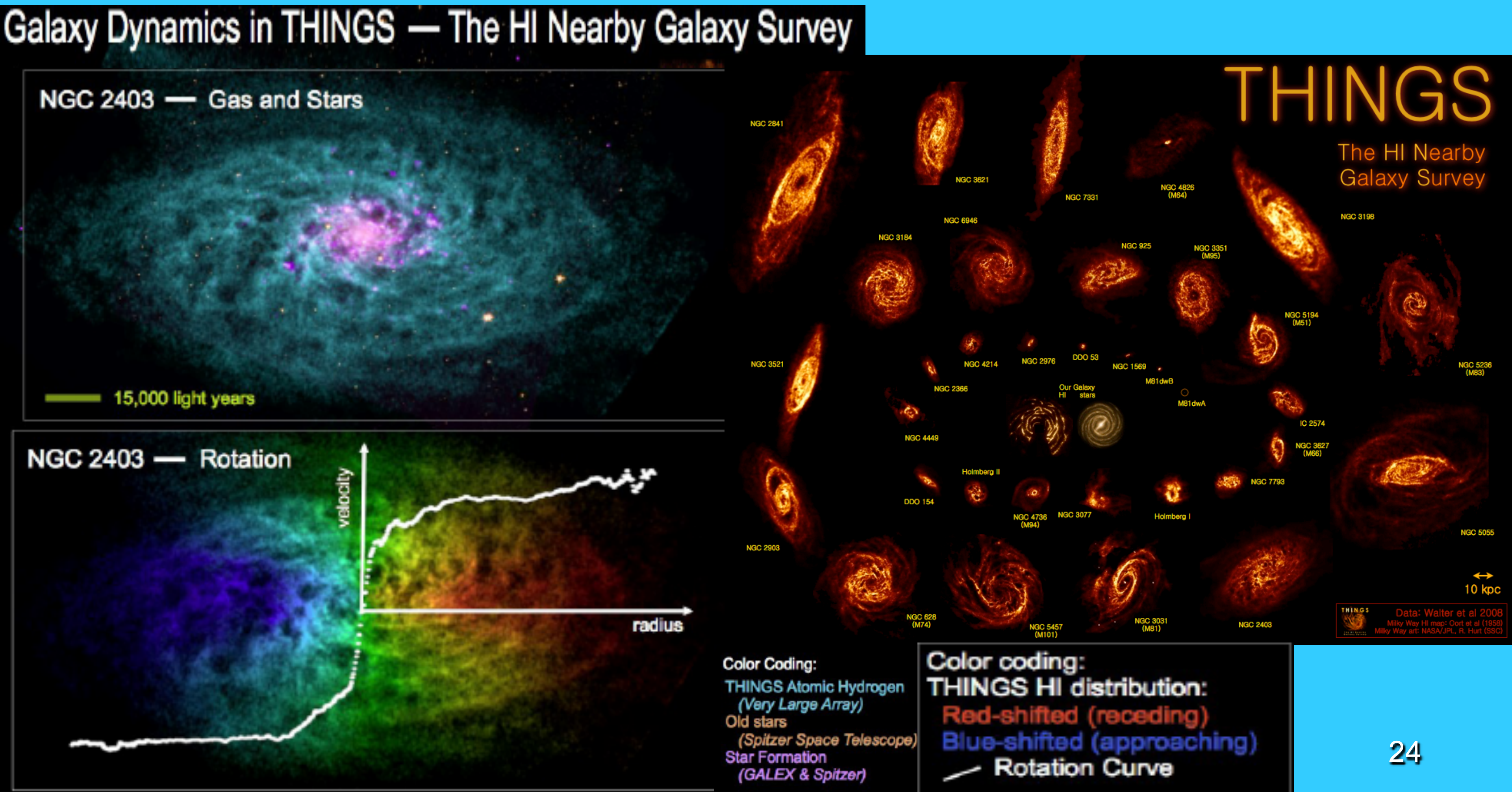

*

Is There a Universal Density Profile?

Adams+2014

Model parameter constraints

	Galaxy	log M_{200} /$M_\odot$	c	γ	β_z	Υ_*	i (°)	PA(°)	v_{sys} (km s^{-1})	$\Delta\alpha_0$ (″)	$\Delta\delta_0$ (″)	σ_{sys} (km s^{-1})
Gas-traced	NGC0959	11.06±0.23	16.7±2.0	0.88±0.15	...	1.10±0.15	55.2±0.1	62.8±1.9	597.0±0.8	0.8±0.4	-0.1±0.5	5.6±0.7
	UGC02259	11.42±0.14	18.2±2.6	0.72±0.09	...	1.07±0.27	41.0±0.2	159.9±1.5	581.6±1.1	-0.8±1.0	1.0±1.2	5.5±0.5
	NGC2552	11.33±0.11	18.1±2.0	0.38±0.11	...	1.01±0.19	52.9±0.1	57.8±0.9	521.9±0.7	0.9±0.8	1.4±0.9	5.7±0.3
	NGC2976	11.94±0.51	20.6±3.3	0.30±0.18	...	0.83±0.22	62.0±0.2	-34.4±1.6	5.3±1.1	-1.3±1.5	-1.5±1.3	6.9±0.4
	NGC5204	11.36±0.16	18.7±2.1	0.85±0.06	...	1.08±0.13	46.8±0.1	171.0±2.2	201.6±0.9	0.2±1.0	-0.8±1.0	6.6±0.7
	NGC5949	11.82±0.42	17.5±1.9	0.53±0.14	...	1.16±0.34	62.0±0.1	148.5±2.0	442.4±1.7	1.2±0.6	0.2±0.7	5.4±0.8
	UGC11707	11.49±0.18	15.1±1.6	0.41±0.11	...	1.11±0.23	72.7±0.1	56.8±1.0	899.4±1.0	1.4±0.7	0.2±0.8	7.5±0.4
Stellar-traced	NGC0959	11.64±0.32	18.5±2.4	0.73±0.10	-0.05±0.20	1.08±0.27	55.3±0.1	65.4±2.2	596.5±2.0	-0.6±2.0	0.4±1.0	3.0±1.1
	UGC02259	11.62±0.61	16.7±5.7	0.77±0.21	0.28±0.39	1.10±0.44	41.1±0.2	157.6±3.3	578.7±2.9	0.9±2.3	-0.6±3.0	3.3±1.2
	NGC2552	11.23±0.38	15.8±3.6	0.53±0.21	0.35±0.29	1.24±0.55	52.8±0.2	56.9±3.1	521.9±2.7	-1.3±2.5	-0.3±2.4	3.6±0.7
	NGC2976	11.56±0.46	17.7±2.5	0.53±0.14	0.49±0.07	0.93±0.21	62.0±0.1	-33.6±3.0	1.5±1.3	0.6±2.3	0.3±1.9	2.3±0.6
	NGC5204	11.76±0.51	18.3±3.3	0.77±0.19	0.65±0.19	1.30±0.42	47.0±0.1	172.6±3.5	201.4±2.2	-0.9±2.4	-1.6±2.7	2.9±1.6
	NGC5949	11.46±0.22	17.5±1.9	0.72±0.11	0.11±0.17	1.20±0.28	62.1±0.1	146.3±1.3	441.3±1.5	-0.5±0.7	-0.1±0.7	2.9±1.1
	UGC11707	11.13±0.37	17.3±4.9	0.65±0.26	0.34±0.26	1.07±0.44	72.8±0.2	53.1±4.0	896.6±3.8	1.0±4.3	0.5±2.9	3.6±1.2

NGC 5963 1.28

- Simon et al. (2005)

- Also different from previous observations, though
  e.g., $\alpha = 0.2 \pm 0.2$ (de Blok, Bosma, & McGaugh 2003)

Diversity in dwarf galaxies density profile

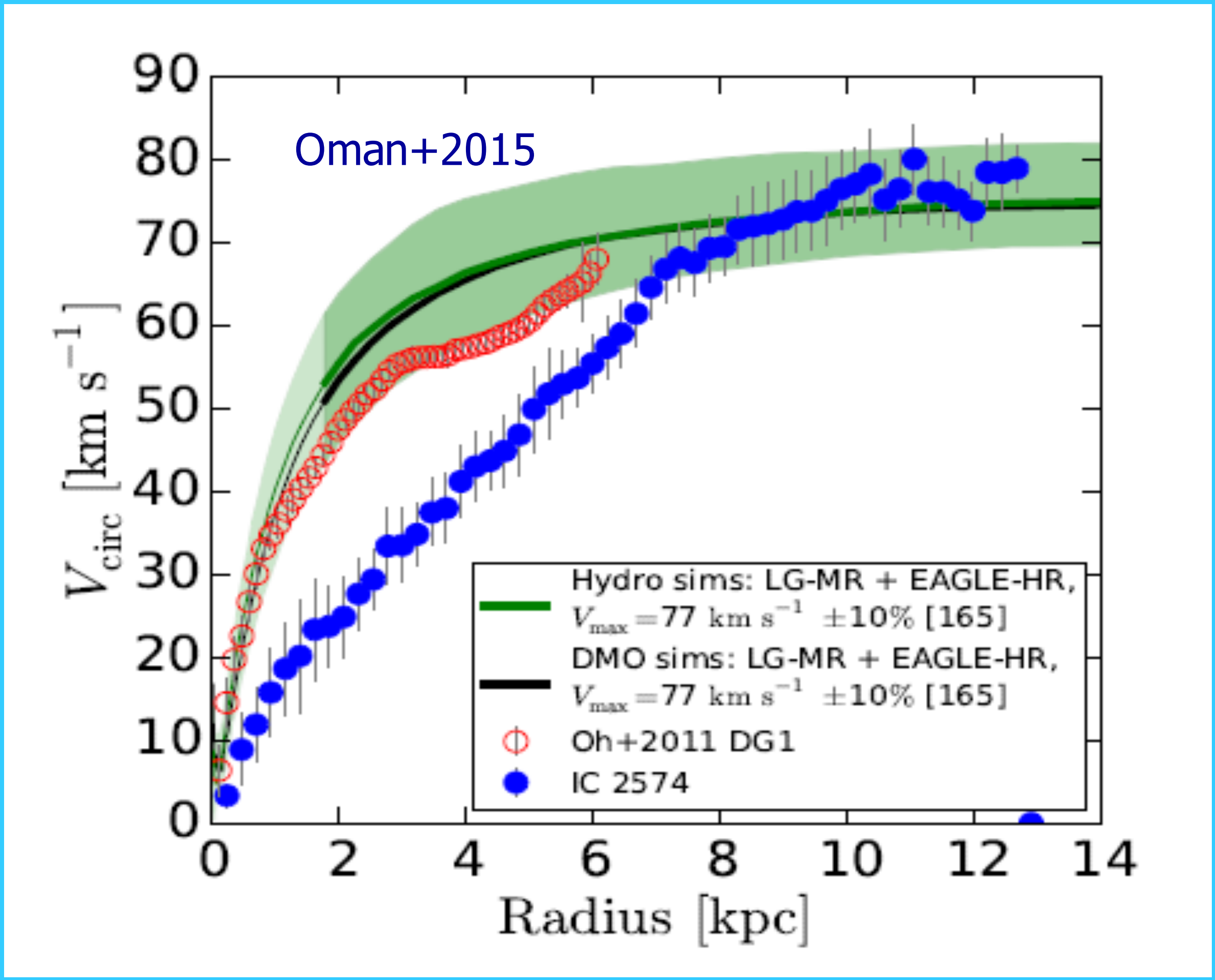

ENVIRONMENT

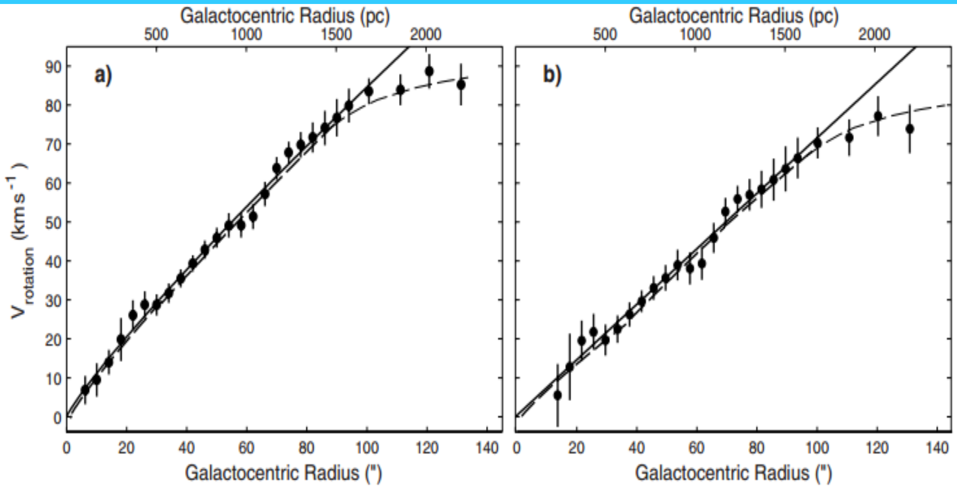

Figure 4. (a) Minimum disc rotation curve of NGC 2976. Black circles with error bars represent the rotation velocities relative to the minimum disc obtained by S03. The solid line is a power-law fit to the rotation curve, which corresponds to a density profile of $\rho \propto r^{-0.27}$, obtained by S03. The dashed line plots the results of the model of this paper. (b) Maximum disc rotation curve of NGC 2976. Similar to (a), except $\rho \propto r^{-0.01}$.

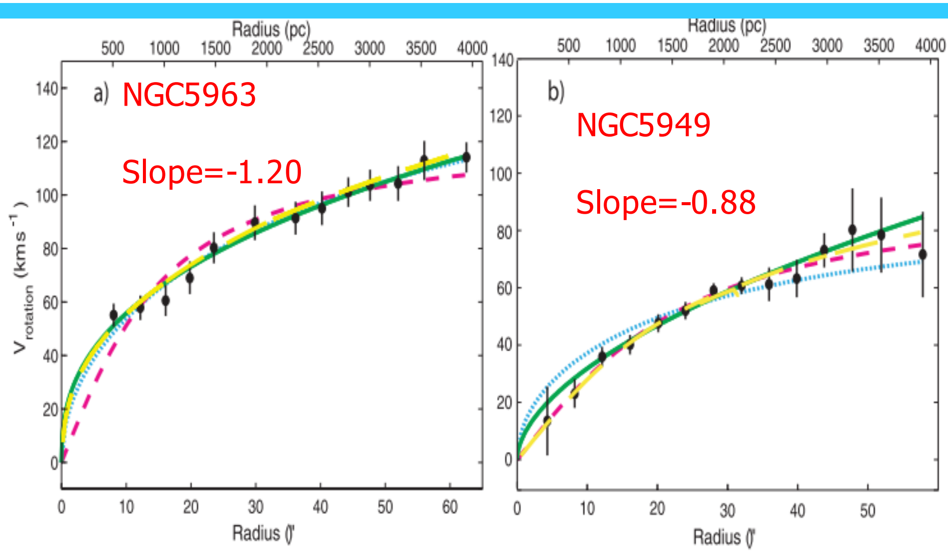

Figure 5. (a) Disc-subtracted rotation curve of NGC 5963. As in Fig. 4, the black points represent the dark matter halo rotation curve, obtained by S05, after subtracting the stellar disc. The solid, dotted and short-dashed lines show the power-law, NFW and pseudo-isothermal fits, respectively, obtained by S05. The long-dashed curve is the dark matter halo rotation curve obtained from the model in this paper. (b) Disc-subtracted rotation curve of NGC 5949. The symbols have the same meanings as in (a).

Table 1. Sample of dwarf (type = 0), LSB (type = 1) and normal spiral (type = 2) galaxies and constraints on the model parameters.

ID	Type	Reference	Θ	α
UGC 1281	1	dBB02	−1.2	$0.92^{+0.08}_{-0.08}$
UGC 8490	0	Sw11[a]	−1.1	$0.89^{+0.06}_{-0.06}$
NGC 4605	0	S05	−1.1	$0.78^{+0.06}_{-0.06}$
M81 dwB	0	Oh10	−0.9	$0.39^{+0.06}_{-0.06}$
NGC 5023	1	dBB02	−0.5	$0.79^{+0.07}_{-0.07}$
NGC 4736	2	dBB02	−0.5	$0.81^{+0.08}_{-0.08}$
NGC 3274	1	dBB02	−0.3	$0.75^{+0.07}_{-0.07}$
NGC 2403	2	dBB02	0	$0.51^{+0.06}_{-0.06}$
UGC 7524	0	Sw11	0.1	$0.46^{+0.06}_{-0.06}$
UGC 7559	0	Sw11	0.1	$0.38^{+0.06}_{-0.06}$
NGC 7793	2	dBB02	0.1	$0.07^{+0.05}_{-0.05}$
Ho II	0	Oh10	0.6	$0.43^{+0.06}_{-0.06}$
DDO 53	0	Oh10	0.7	$0.38^{+0.06}_{-0.06}$
IC 2574	0	dBB02	0.9	$0.09^{+0.07}_{-0.07}$
NGC 2366	0	dBB02	1.0	$0.32^{+0.1}_{-0.1}$
Ho I	0	Oh10	1.5	$0.38^{+0.06}_{-0.06}$
NGC 2976	0	dBB02	2.7	$0.01^{+0.1}_{-0.1}$

[a]Swaters et al. (2011)

$$\Theta = \max\left[\log\left(\frac{M_k}{D_k^3}\right)\right] + C,$$

Del Popolo 2012,
Del Popolo & Cardone 2012

SPIRALS: WHAT WE KNOW

MORE PROPORTION OF DARK MATTER IN SMALLER SYSTEMS

MASS PROFILE AT LARGER RADII COMPATIBLE WITH NFW

DARK HALO DENSITY SHOWS OFTEN A CENTRAL CORE OF SIZE 2 R_D

ISO HALOS OFTEN PREFEREED OVER NFW

ELLIPTICALS

Relatively featureless spheroidal galaxies

The Stellar Spheroid

Surface brightness follows a Sersic (de Vaucouleurs) law

$$I(R) = I_e e^{-b_n[(R/R_e)^{1/n}-1]}$$

for n=4 $\ln I(R) = \ln I_e + 7.669\left[1 - \left(\frac{R}{R_e}\right)^{1/4}\right]$

R_e : the effective radius, n Sersic index (light concentration)

By deprojecting I(R) we obtain the luminosity density j(r):

$$I(R) = \int_{-\infty}^{+\infty} j(r)\, dz = 2\int_{R}^{+\infty} \frac{j(r)\, r\, dr}{\sqrt{r^2 - R^2}}$$

Assuming radially constant stellar mass to light ratio

$$\rho_{sph}(r) = (M/L)_\star\, j(r)$$

Kinematics of ellipticals: Jeans modelling of radial, projected and aperture velocity dispersions

$$M(r) = M_{sph}(r) + M_h(r).$$

$$\sigma_r^2(r) = \frac{G}{\rho_{sph}(r)} \int_r^\infty \frac{\rho_{sph}(r')M(r')}{r'^2}\, dr'$$

Radial

$$\sigma_P^2(R) = \frac{2}{I(R)} \int_R^\infty \frac{\rho_{sph}(r)\ \sigma_r^2(r)\ r}{\sqrt{r^2 - R^2}}\, dr$$

Projected (los)

$$\sigma_A^2(R_A) = \frac{2\pi}{L(R_A)} \int_0^{R_A} \sigma_P^2(R)\ I(R)\ R\ dR$$

Aperture

$$L(R) = 2\pi \int I(R)\ R\ dR$$

When observed through an aperture of finite size, the projected velocity dispersion profile, σp is weighted on the brightness profile I(R).

-Rotation is not always negligible
-σ_r (R) is a direct probe of grav potential but it is not observable
-σ_P (R) is observable when individual star measures are available

measure I(R), σ_P(R)

derive M_h(r), M_{sph}(r)

Modelling Ellipticals

- Measure the light profile= stellar mass profile $(M_*/L)^{-1}$
- Derive the total mass M(r) profile from
- -Virial theorem
- -Dispersion velocities of kinematical tracers (e.g., stars, Planetary Nebulas)
- Disentangle M(r) into its dark and the stellar components. **In ellipticals gravity is balanced by pressure gradients -> Jeans Equation**

$$\frac{1}{\rho}\frac{d(\rho\sigma_r^2)}{dr} + 2\frac{\beta\sigma_r^2}{r} = -\frac{d\phi}{dr}$$

or

$$\frac{\mathrm{d}(\ell\sigma_r^2)}{\mathrm{d}r} + 2\,\frac{\beta(r)}{r}\,\ell\sigma_r^2 = -\ell(r)\,\frac{GM(r)}{r^2}$$

Spherical Symmetry; Non-rotating system

L(r) luminosity density

$$\beta \equiv 1 - \frac{\sigma_\theta^2}{\sigma_r^2}$$

Velocity dispersion anisotropy

- Difficulties in inferring the presence of dark matter halos in ellipticals:

1) the velocity dispersions of the usual kinematical tracer, stars, can only be measured out to $2R_e$.
2) Mass/anisotropy degeneracy: For a given $\rho(r)$, $\sigma_r(r)$, two unknown remains: M(r), and $\beta(r)$ and one cannot solve Jeans equation for both, unless one assumes no rotation and makes use of the 4th order moment (kurtosis) of the velocity distribution (Lokas & Mamon 2003).

(One of the first studies Romanowsky et al. 2003-> a dearth of DM in E)

-X-ray properties of the emitting hot gas

-Combining weak and strong lensing data

*

Jeans modelling using PN

Pseudo inversion mass model

Napolitano et al. (2011)

(i) Adopt a simple smooth parametric function for the intrinsic radial velocity dispersion profile:

$$\sigma_r(r) = \sigma_0 \left[1 + \left(\frac{r}{r + r_0}\right)^{\eta}\right]^{-1}, \quad (2)$$

where σ_0, r_0, η are a minimalistic set of free parameters.

(ii) Assume a given anisotropy profile, often constant or parametrized as a simple function:

$$\beta(r) \equiv 1 - \sigma_\theta^2/\sigma_r^2, \qquad \beta(\xi) = \beta_0 \frac{\xi^{1/2}}{\xi^2 + 1},$$

$\beta_0 = 0.6$ and $\xi = r/r_a$ with $r_a \sim 30$ arcsec

(iii) Project the line-of-sight components of the 3D velocity dispersions σ_r and σ_θ for comparison with the line-of-sight velocity dispersion data $\sigma_{los}(R)$.

(iv) Iteratively adjust the free parameters in equation (2) to best fit the model to the observed dispersion profile.

(v) Use the best-fitting model (equation 2) in the Jeans equation

[redacted]

$$M(r) = -\frac{\sigma_r^2 r}{G}\left(\frac{d\ln j_*}{d\ln r} + \frac{d\ln \sigma_r^2}{d\ln r} + 2\beta\right),$$

where $j_*(r)$ is the spatial density of the PNe

Multicomponent model

(0) Parametrized mass profile, e.g. NFW

(i) Set up a multi-dimensional grid of model parameter space to explore, including β and the mass profile parameters $(\Upsilon_*, \rho_s, r_s)$ or (Υ_*, v_0, r_0).

(ii) For each model grid-point, solve the 2nd- and 4th-order Jeans equations.

(iii) Project the internal velocity moments to σ_{los} and κ_{los}.

$$\kappa \equiv \overline{v^4}/(\overline{v^2})^2 - 3$$

(iv) Compute the χ^2 statistics, defined as

$$\chi^2 = \sum_{i=1}^{N_{data}} \left[\frac{p_i^{obs} - p_i^{mod}}{\delta p_i^{obs}}\right]^2, \quad (16)$$

where p_i^{obs} are the observed data points (σ_{los} and κ_{los}), p_i^{mod} the model values, and δp_i^{obs} the uncertainties on the observed values, all at the radial position R_i.

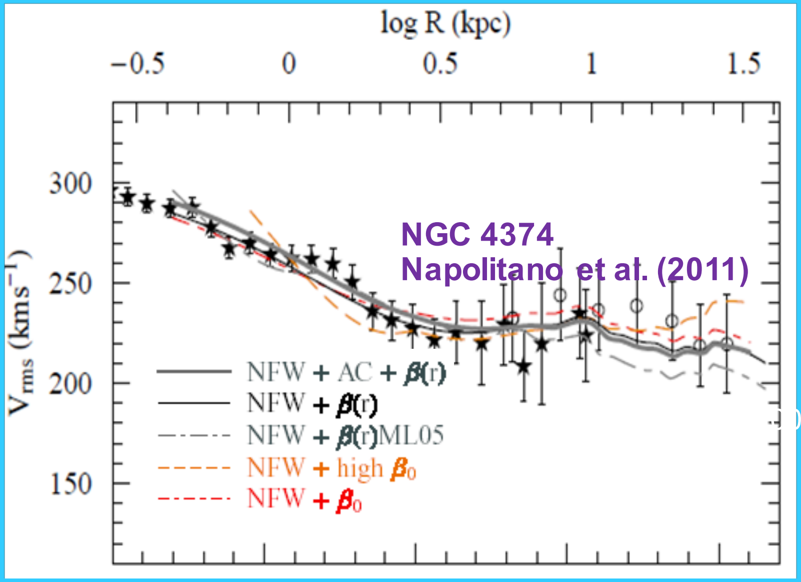

05

Ellipticals have big DM halos (usually cuspy profiles, sometime cored

Jeans modelling of PN data with a stellar spheroid + NFW dark halo

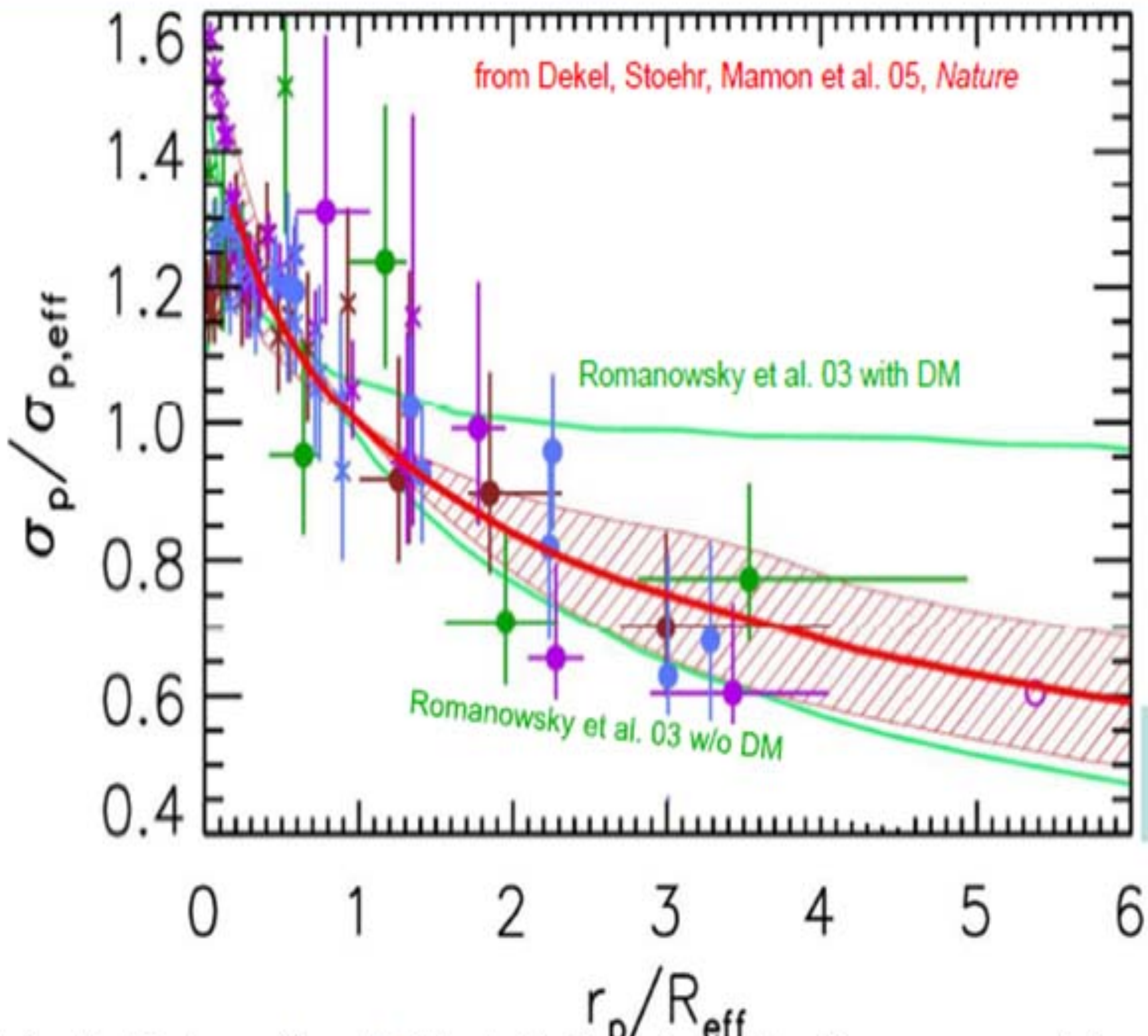

Observed (symbols) and simulated (red curve) line-of-sight velocity dispersion profiles. Green curves predictions of Romanowsky et al. (03), without and with dark matter. The simulations (by T. J. Cox) are binary mergers of spirals made of disk +bulge + gas + dark-matter-halo. Red curve: mean line-of-sight velocity dispersion profile for the elliptical galaxy remnant, averaged over 10 simulations with different orbital parameters. Hashed: dispersion over the 10 simulations. The plot indicates that one can have strongly decreasing line-of-sight velocity dispersion profiles despite the presence of dark matter. PNs (circles) and stars (crosses) of the galaxies studied by Romanowsky are marked green (NGC 821), violet (NGC 3379), brown (NGC 4494) and blue (NGC 4697) with 1σ errors. Green lines: earlier models with (upper) and without DM

Dark-Luminous mass decomposition of dispersion velocities

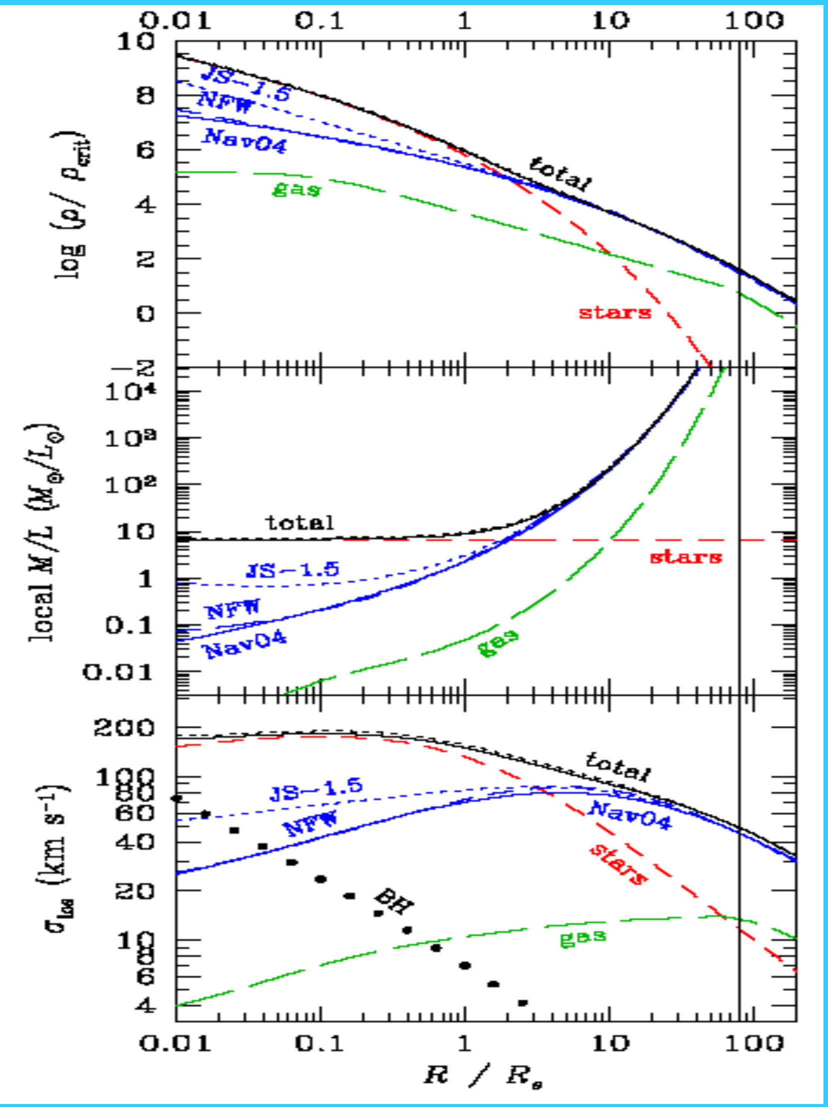

$M_{vir} = 2 \times 10^{12} M_\odot \quad M_{sph} = 1 \times 10^{12} M_\odot \quad R_e = \ 3\ kpc \quad n = 3$

Assumed Isotropy_Three components: DM, stars (Sersic), Black Holes

Naive superposition of Sersic models for the stellar mass component of L=L* elliptical galaxies with hot gas (from X rays) and central black hole (from the Magorrian relation), plus Dark Matter models: NFW; Jing & Suto; Einasto (Nav04). No adiabatic contraction.

Mamon & Łokas 05

This plot indicates that while dark matter dominates outside of a few Re, the stellar component dominates inside Re. Therefore, it is difficult to measure the amount of dark matter in the inner regions of ellipticals.

The spheroid determines the velocity dispersion

Stars dominate inside R_e

Dark matter profile "unresolved"

ELLIPTICALS: WHAT WE KNOW

A LINK AMONG THE STRUCTURAL PROPERTIES OF STELLAR SPHEROID

SMALL AMOUNT OF DM INSIDE R_E

MASS PROFILE COMPATIBLE WITH NFW AND BURKERT?

DARK MATTER DIRECTLY TRACED OUT TO R_{VIR}

Dwarf spheroidals: basic properties

The smallest objects in the Universe, benchmark for theory

$$L = 2\times 10^3 L_\odot - 2\times 10^7 L_\odot \quad \sigma_0 \sim 7-12\,\mathrm{km\,s^{-1}} \quad r_0 \approx 130-500\,\mathrm{pc}$$

Discovery of ultra-faint MW satellites (e.g. Belokurov et a. 2007), extends the range of dSph structural parameters: 1 order of magnitude in radius and 3 in luminosity

1. Apparently in equilibrium
2. Small number of stars
3. No dynamically significant gas

dSph show large M_{grav}/L 10-100)

Luminosities and sizes of Globular Clusters and dSph are different

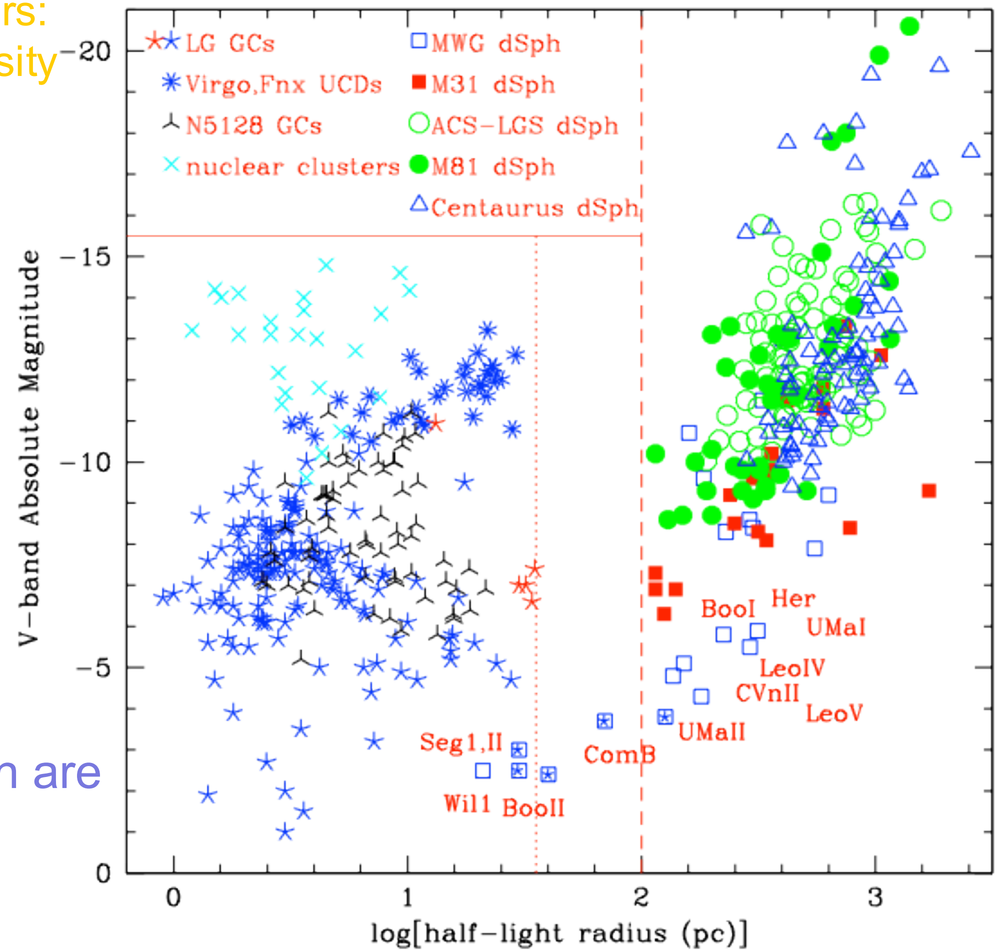

Gilmore et al 2009

dSphs Dispersion velocity profiles

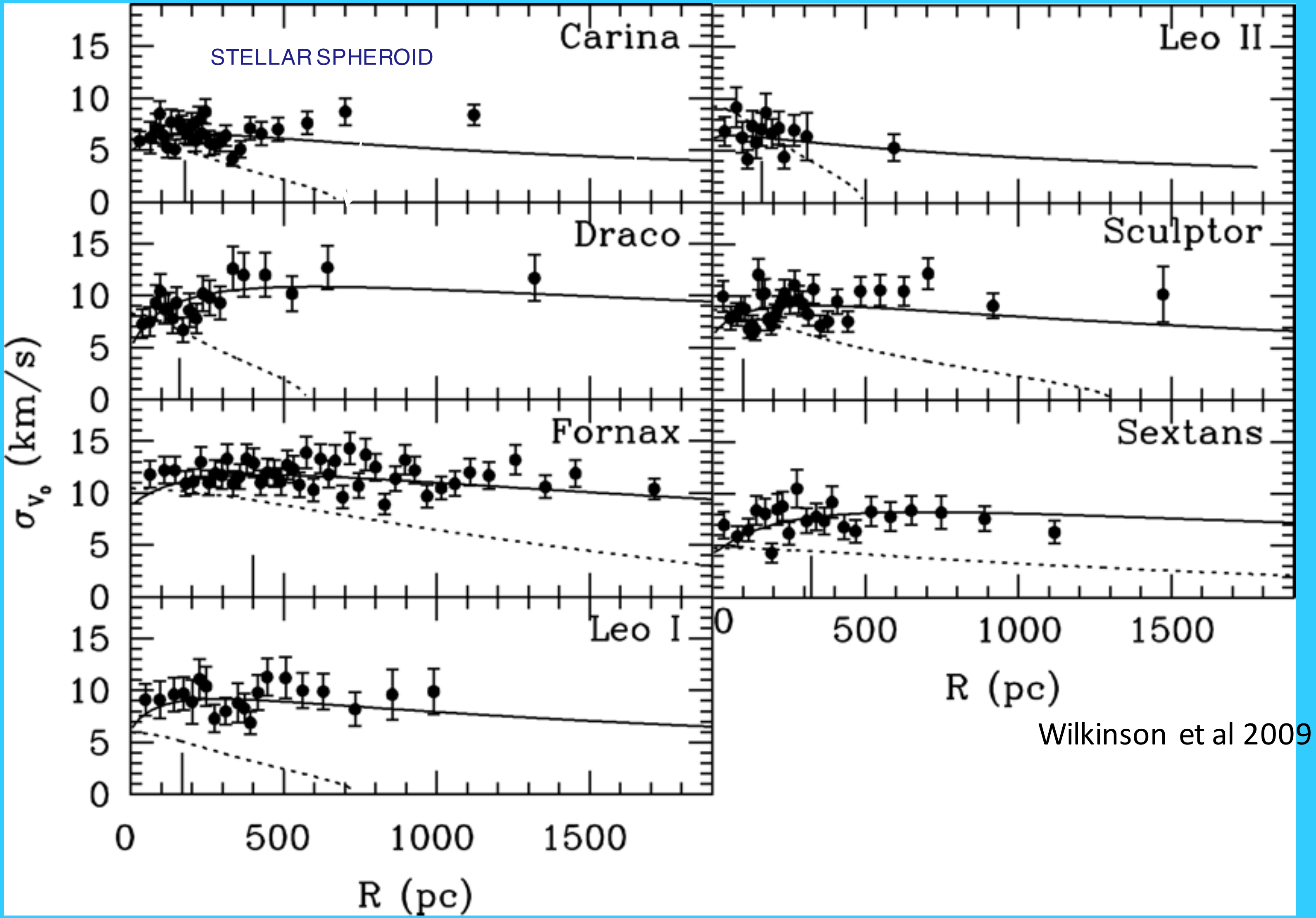

dSph dispersion profiles generally remain flat to large radii

Mass profiles of dSphs

- In a collisionless equilibrium systems, Jeans equation relates kinematics, light and underlying mass distribution
- Make assumptions on the velocity anisotropy and then fit the dispersion profile-> DM mass distribution

$$M(r) = -\frac{r^2}{G}\left(\frac{1}{\nu}\frac{\mathrm{d}\,\nu\sigma_r^2}{\mathrm{d}\,r} + 2\,\frac{\beta\sigma_r^2}{r}\right)$$

- The surface brightness profiles are typically fit by a Plummer distribution (Plummer 1915)

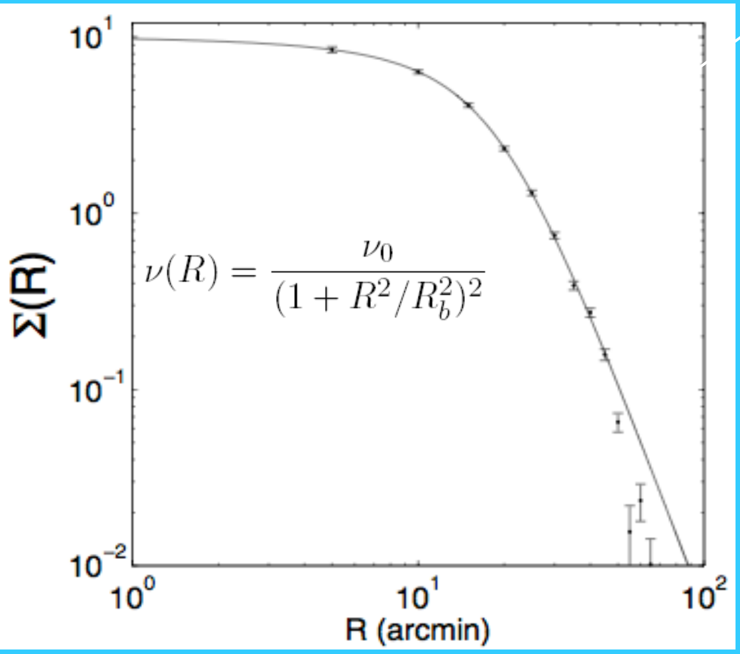

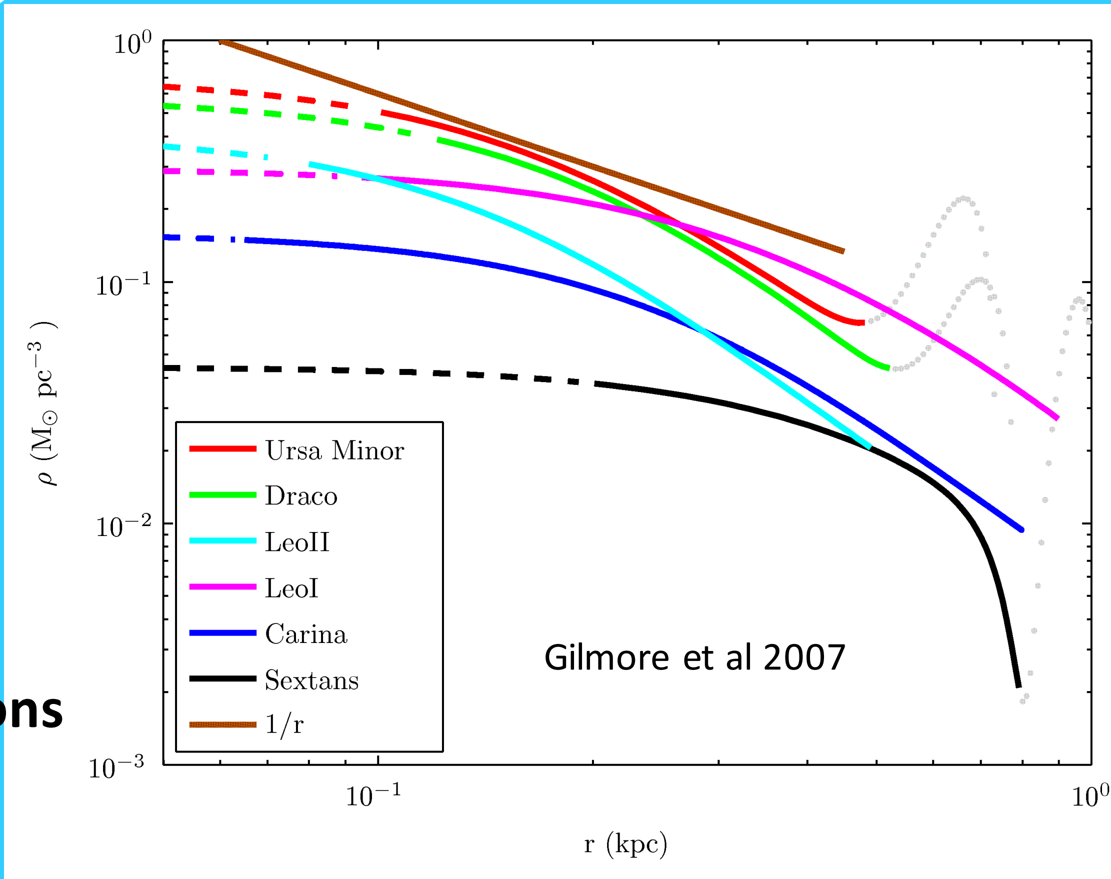

Results point to cored distributions

Degeneracy between DM mass profile and velocity anisotropy

- Dispersion velocity profiles remain generally flat to large radius
- Cored and cusped halos with orbit anisotropy fit dispersion profiles equally well

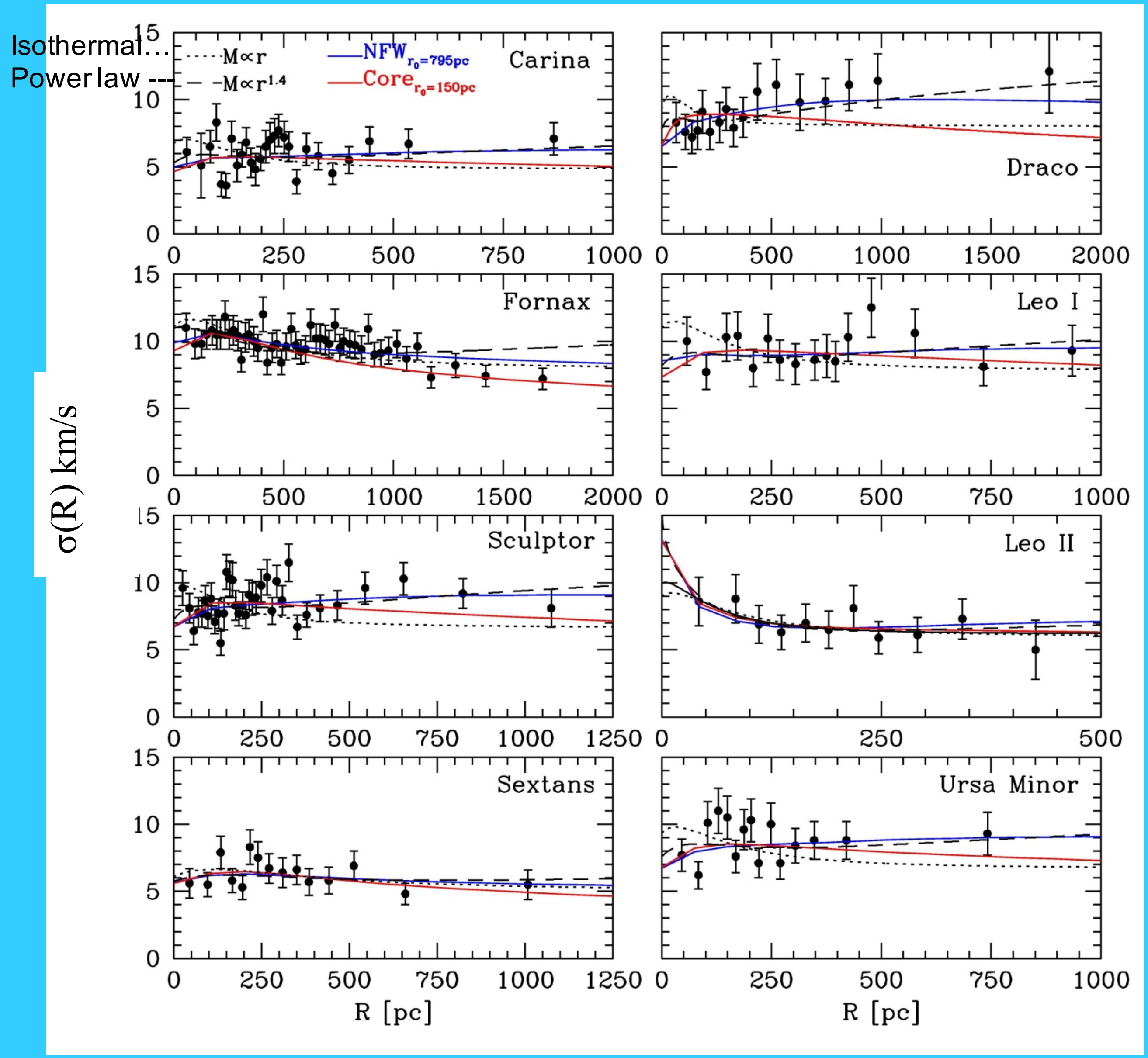

Walker et al 2009

dSphs may all have a universal density profile (e.g., Walker et al. 2009), and that they may not (e.g., Collins et al. 2013).

Cusp or Core?

Gilmore et al. (2007) favor a cored DM profile

Kleyna et al. (2003): N-body simulations-> Ursa Minor dSph would survive for less than 1 Gyr if the DM core were cusped.

Magorrian (2003):
α= 0.55(+0.37, -0.33)
for the Draco dSph.

Fornax and Sculptor-> core (Jardel & Gebhardt 2012; Jardel et al. 2013; Jardel & Gebhardt 2013; Breddels et al. 2013)
BUT
CUSP: (Strigari et al. 2010; Breddels & Helmi 2013).

DSPH: WHAT WE KNOW

PROVE THE EXISTENCE OF DM HALOS OF 10^{10} M_{SUN} AND ρ_0 =10-^{21} g/cm^3

DOMINATED BY DARK MATTER AT ANY RADIUS

HINTS FOR THE PRESENCE OF A DENSITY CORE ?

Density Profiles of Galaxy Clusters

Galaxy Clusters

- Half of all galaxies are in clusters (higher density; more Es and S0; mass > few times 10^{14}-10^{15}) or groups (less dense; more Sp and Irr; less than $10^{14} M_{sun}$)
- 100s to 1000s of gravitationally bound galaxies
- Typically ~few Mpc across
- Central Mpc contains 50 to 100 luminous galaxies ($L > 2 \times 10^{10} L_{sun}$)
- Distribution of galaxies falls as r ¼ (like surface brightness of elliptical galaxies)

Coma Cluster

Measuring DM content in clusters

- Gravitational lensing: measure mass without regard to the dynamical state of the cluster. Cannot distinguish between light and dark mass components, another mass tracer is needed to disentangle luminous from dark matter
- Typical structures observed in the strong lensing regime are radial arcs, located in positions corresponding to the local derivative of the cluster mass density profile, and tangential arcs, the position of which is determined by the projected mass density interior to the arc

- Dynamics (similar to the Ellipticals case)

  - cluster galaxies (or stars of the BCG) as tracers of the potential.

$$\frac{d\rho_*(r)\sigma_r^2(r)}{dr} + \frac{2\alpha(r)\rho_*(r)\sigma_r^2(r)}{r} = -\frac{GM_{enc}(r)\rho_*(r)}{r^2}$$

$$\alpha(r) \equiv 1 - \frac{\sigma_\theta^2(r)}{\sigma_r^2(r)} \equiv \frac{r^2}{r^2 + r_a^2}$$

Osipkov-Merrit parameterization of the anisotropy

$$\sigma_r^2(r) = \frac{G\int_r^\infty dr'\rho_*(r')M_{enc}(r')\frac{r_a^2+r'^2}{r'^2}}{(r_a^2 + r^2)\rho_*(r)}$$

$$\sigma_p^2(R) = \frac{2}{(M_*/L)I(R)}\int_R^\infty dr'\left[1 - \frac{R^2}{r_a^2 + r'^2}\right]\frac{\rho_*(r')\sigma_r^2(r')r'}{(r'^2 - R^2)^{1/2}}$$

- X-Ray emission of ICM

X-Ray in Ellipticals and Clusters

- First detection around M87 in Virgo (Byram et al. 1966; Bradt et al. 1967)
- 1971: detection in Coma and Perseus (Fritz et al. 1971; Gursky et al. 1971)

For an ideal gas, $P = \frac{\rho}{\mu m_{\rm H}} kT$.

The equation of hydrostatic equilibrium is: $\frac{\mathrm{d}P}{\mathrm{d}r} = -\frac{GM}{r^2}\rho$.

So $M(r) = \frac{k}{G\mu m_{\rm H}} \frac{r^2}{\rho} \left(-T\frac{\mathrm{d}\rho}{\mathrm{d}r} - \rho\frac{\mathrm{d}T}{\mathrm{d}r}\right) = \frac{kT}{\mu m_{\rm H}} \frac{r}{G} \left(-\frac{\mathrm{d}\ln\rho}{\mathrm{d}\ln r} - \frac{\mathrm{d}\ln T}{\mathrm{d}\ln r}\right)$.

Therefore if an X-ray telescope provides $\rho(r)$ and $T(r)$ for the *gas*, then we can infer the *total* mass distribution $M(r)$.

IF: 1) isothermal spherical gas cloud in hydrostatic equilibrium
2) volume density of galaxies King profile-> density profile of X-ray emitting gas ~ isothermal β model

β model $$\rho_{gas}(r) = \rho_0 \left(1 + \left(\frac{r}{R_c}\right)^2\right)^{-\frac{3}{2}\beta}$$

Parameters determined by analysis of the X-ray surface brightness profile obtained from X-ray image analysis and well approximated by

$$S(r) = S_0 \left(1 + \left(\frac{r}{R_c}\right)^2\right)^{-3\beta+\frac{1}{2}} + C$$

The equation for M(r) can be applied to either galaxies or clusters but T(r) is more straightforward to measure in clusters. The main complication is lack of spherical symmetry.

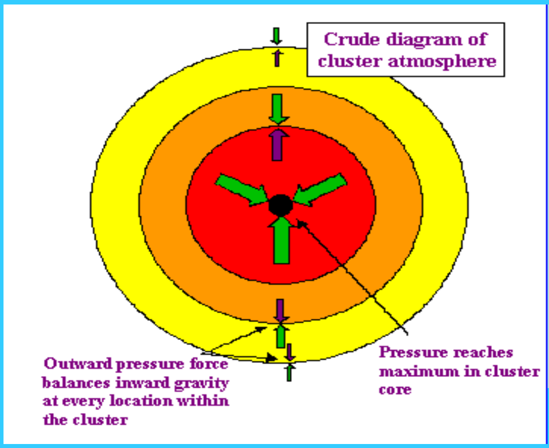

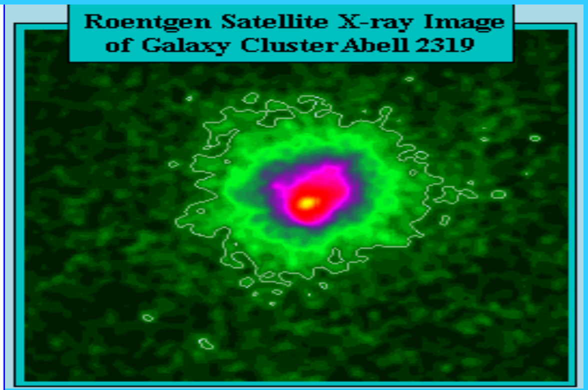

T = 10^6 K → X-ray emission

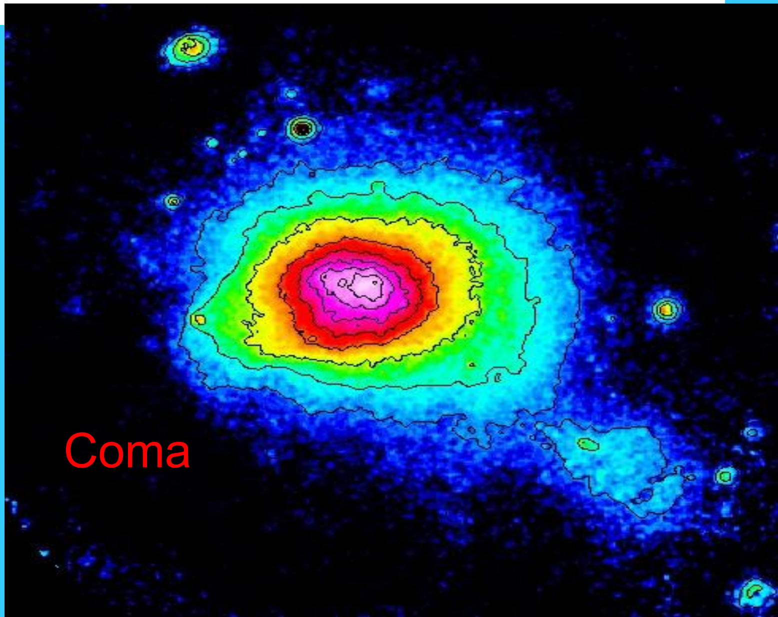

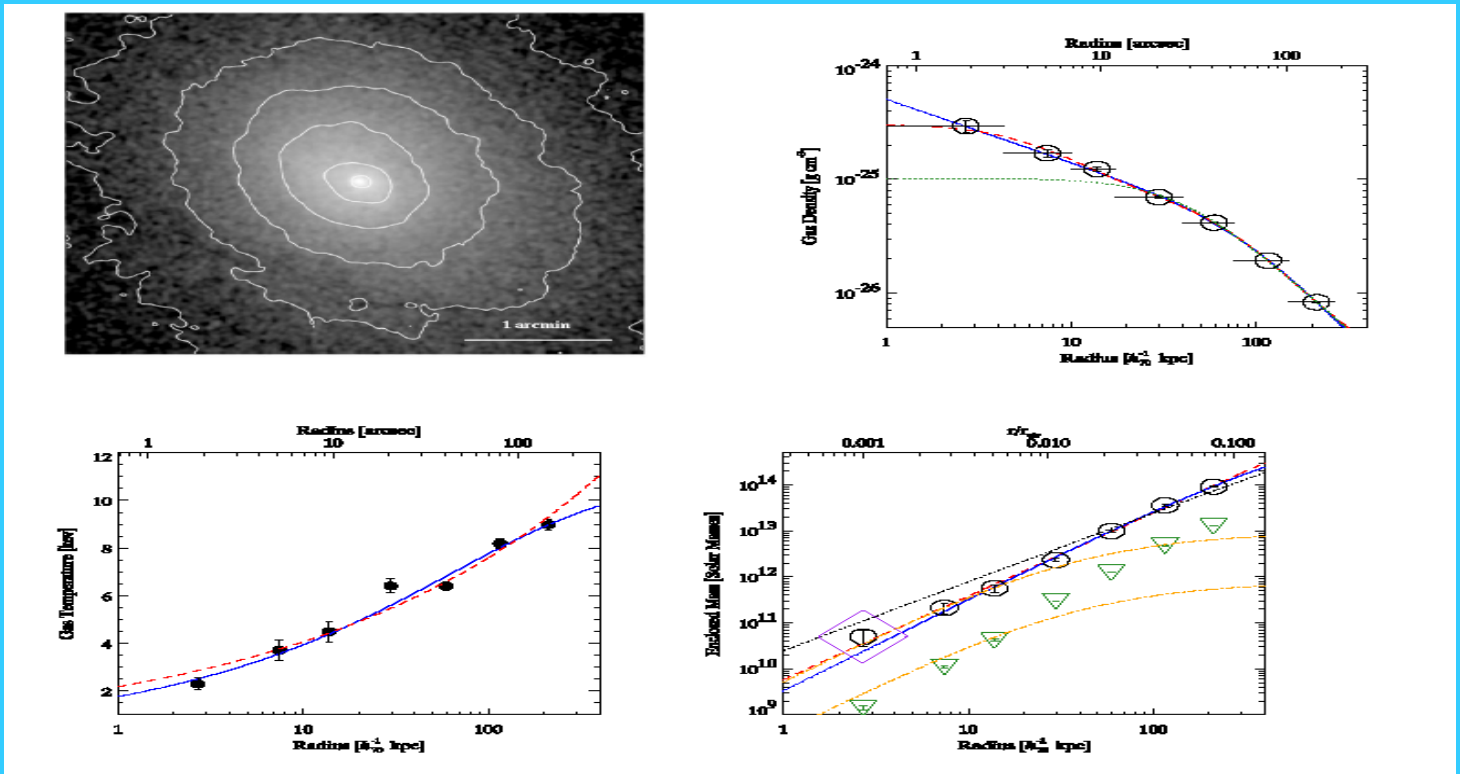

Figures illustrating the basic observables and results typical for X-ray analyses of cluster mass distributions. Typically, the X-ray image is split up into a series of circular, concentric annuli, with the spectrum of each annulus compared to a plasma model to infer the gas density and temperature.

Top Left.Chandra image of Abell 2029. Top Right.Radial gas density profile of Abell 2029 (large circles) fit to several standard parameterizations. This parameterized fit is then fed into equation for M(r), along with the temperature profile to calculate the enclose mass profile.

Bottom Left. The radial temperature profile of Abell 2029, again fit to a standard paramaterization to facilitate the hydrostatic equilibrium analysis.

Bottom Right. Total enclosed cluster mass profile. The open circles are the data points and the lines are fits to the data, with the NFWprofile being a very good fit.

The upside down triangles show the contribution from the cluster gas mass. Note that the bright yellow band shows the possible contribution from the cluster BCG,illustrating the need for an additional technique to account for and disentangle this important mass component in order to understand the dark matter density pro.le. This .gure has been reproduced from Lewis et al. (2002, 2003

Mass profiles from XMM-Newton

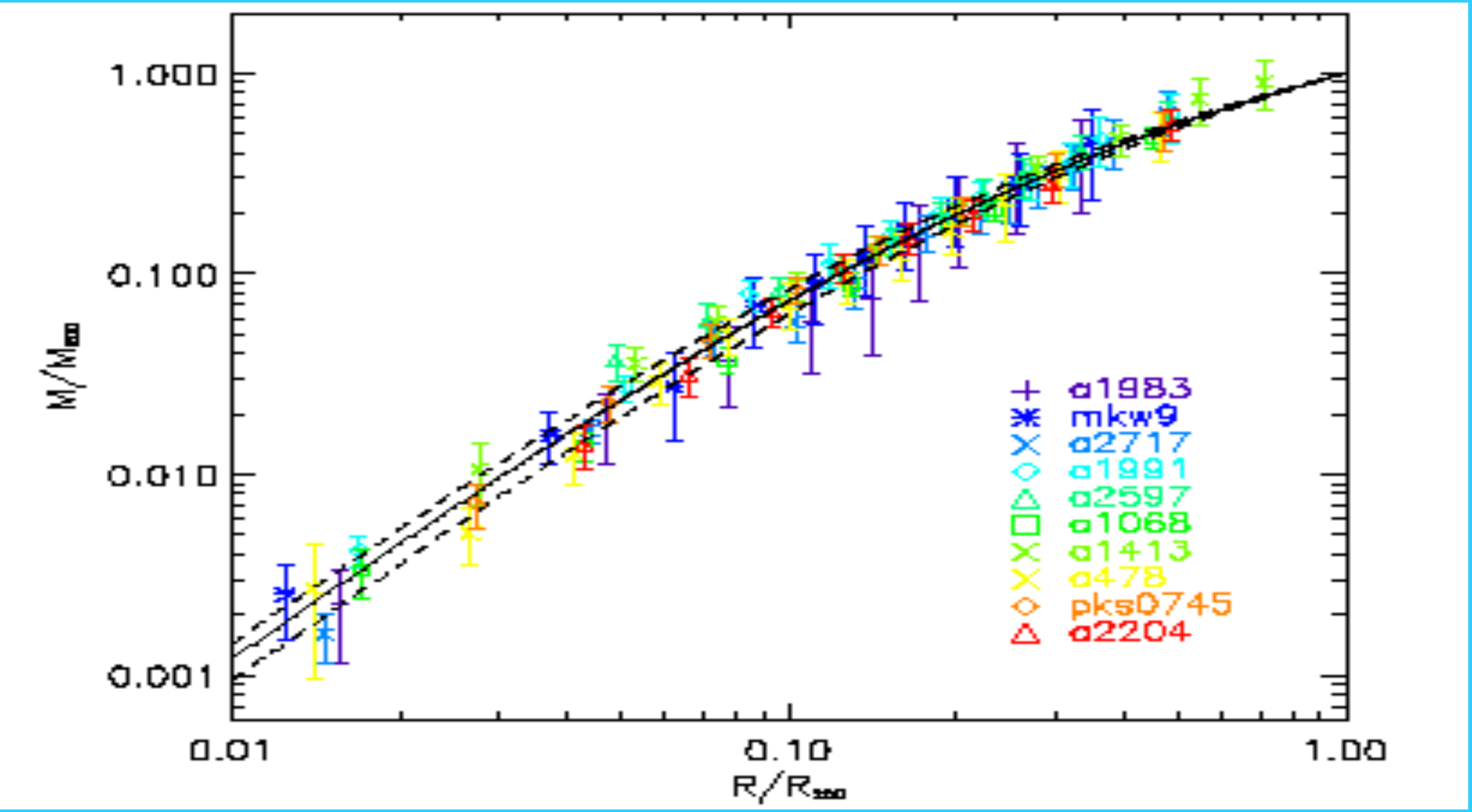

Scaled mass profiles of all clusters. The mass is scaled to *M*200, and the radius to *R*200, both values being derived from the best fitting NFWmodel. The solid black line corresponds to the mean scaled NFWprofile and the two dashed lines are the associated standard deviation.

Limits of X-ray mass determination

- X-ray data alone have difficulties in constraining the mass distribution, especially in the central regions, since relaxed clusters tend to have "cooling flows", and in these clusters X-ray emission is often disturbed and the assumption of hydrostatic equilibrium is questionable (see Arabadjis, Bautz & Arabadjis 2004).

- X-ray analyses, ALONE, cannot disentangle the DM and baryonic components

- X-ray temperature measurements are carried out from 500 kpc (Bradˇac et al. 2008) to 50 kpc. Determination of temperature at smaller radia are limited by instrumental resolution or substructure (Schmidt & Allen 2007).

- Complicated to take account of the stellar mass contained in the BCG (brightest cluster galaxy), located in the cluster center

- X-ray analyses have obtained wide ranging values of the inner slope, of the density profile with ranging from 0.6 (Ettori et al. 2002) through 1.2 (Lewis, Buote & Stocke 2003) to 1.9 (Arabadjis, Bautz & Garmire 2002), while Chandra and XMM-Newton results suggest good agreement with CDM predictions (see Schmidt & Allen 2007, and references therein).

Gravitational Lensing

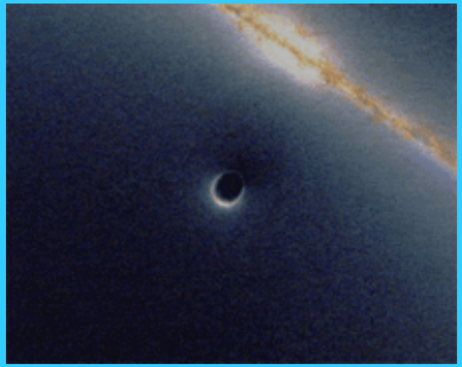

- Bending of light-rays passing through a gravitational field.

- Three classes: strong, weak, micro

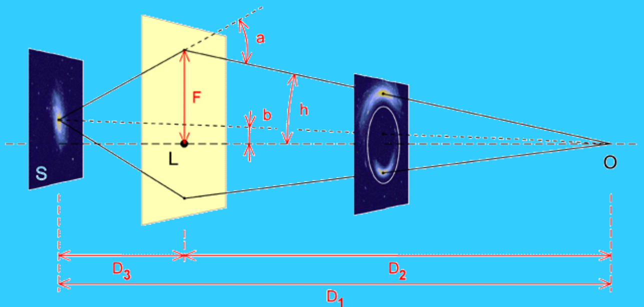

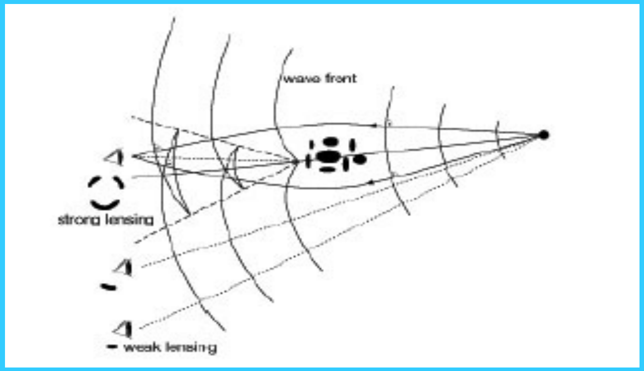

- *Strong Lensing:* the photons move along geodesics in a strong gravitational potential which distorts space as well as time, causing larger deflection angles. Original light source may appear as a ring around the massive lensing object (Einstein Ring)

…otherwise arc segment

Weak Lensing: deflection through a small angle when the light ray can be treated as a straight line (**see figures**), and the deflection as if it occurred discontinuously at the point of closest approach. The shape distortion of background galaxies due to a foreground object (cluster) is used to determine the mass of the object (cluster) independent of dynamical assumptions.

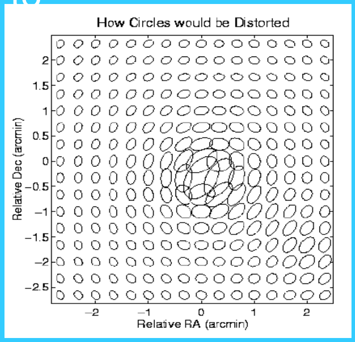

- *Microlensing* if the mass of the lensing object is very small, one will merely observe a magnification of the brightness of the lensed object.

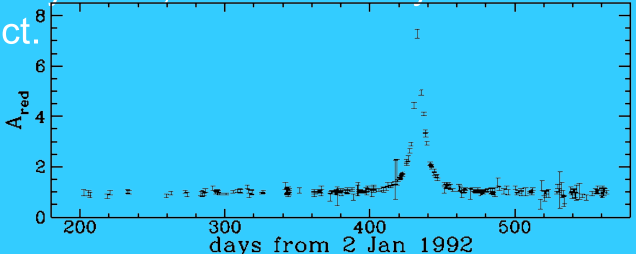

Gravitational Lensing formalism

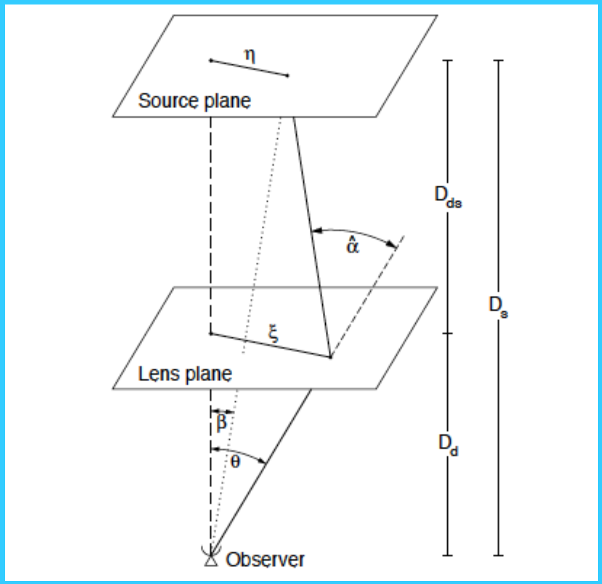


Galaxy Cluster Abell 2218 HST • WFPC2
NASA, A. Fruchter and the ERO Team (STScI) • STScI-PRC00-08

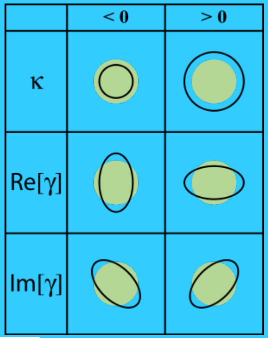

Deflection angle
$$\alpha = \frac{4GM}{c^2\xi} = \frac{4\pi\langle v_{\|}^2\rangle}{c^2}$$

The deflection angle $\vec{\alpha}$ relates a point in the source plane $\vec{\beta}$ to its image(s) in the image plane $\vec{\theta}$ through the lens equation $\vec{\beta} = \vec{\theta} - \vec{\alpha}(\vec{\theta})$

Convergence
$$\kappa(\vec{\theta}) = \frac{\Sigma(D_d\vec{\theta})}{\Sigma_{cr}} \qquad \Sigma_{cr} = \frac{c^2 D_s}{4\pi G D_{ds} D_d}$$
$$\Sigma(\vec{\xi}) = \int \rho(\vec{\xi}, z)dz$$

Angular radius and mass of an Einstein ring
$$\theta_E = \alpha\frac{D_{ds}}{D_s} \qquad M_E = \theta_E^2 \frac{c^2}{4G}\frac{D_d D_{ds}}{D_s}$$

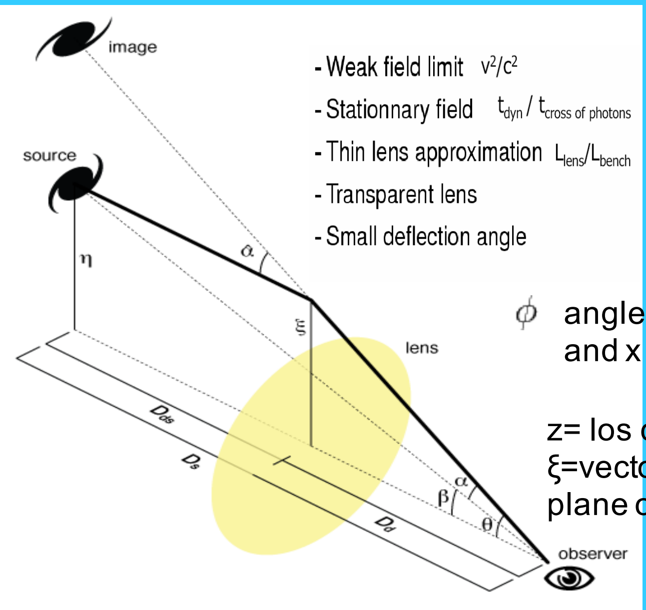

ϕ angle between $\vec{\alpha}$ and x

z= los coordinate
ξ=vector in the plane of sky

Jacobian between the unlensed and lensed coordinate systems
$$A_{ij} = \frac{\partial\beta_i}{\partial\theta_j} = \delta_{ij} - \frac{\partial\alpha_i}{\partial\theta_j} = \delta_{ij} - \frac{\partial^2\psi}{\partial\theta_i\partial\theta_j}$$
$$A = (1-\kappa)\begin{bmatrix}1 & 0\\ 0 & 1\end{bmatrix} - \gamma\begin{bmatrix}\cos 2\phi & \sin 2\phi\\ \sin 2\phi & -\cos 2\phi\end{bmatrix}$$

The term involving the convergence magnifies the image by increasing its size while conserving surface brightness. The term involving the shear stretches the image tangentially around the lens

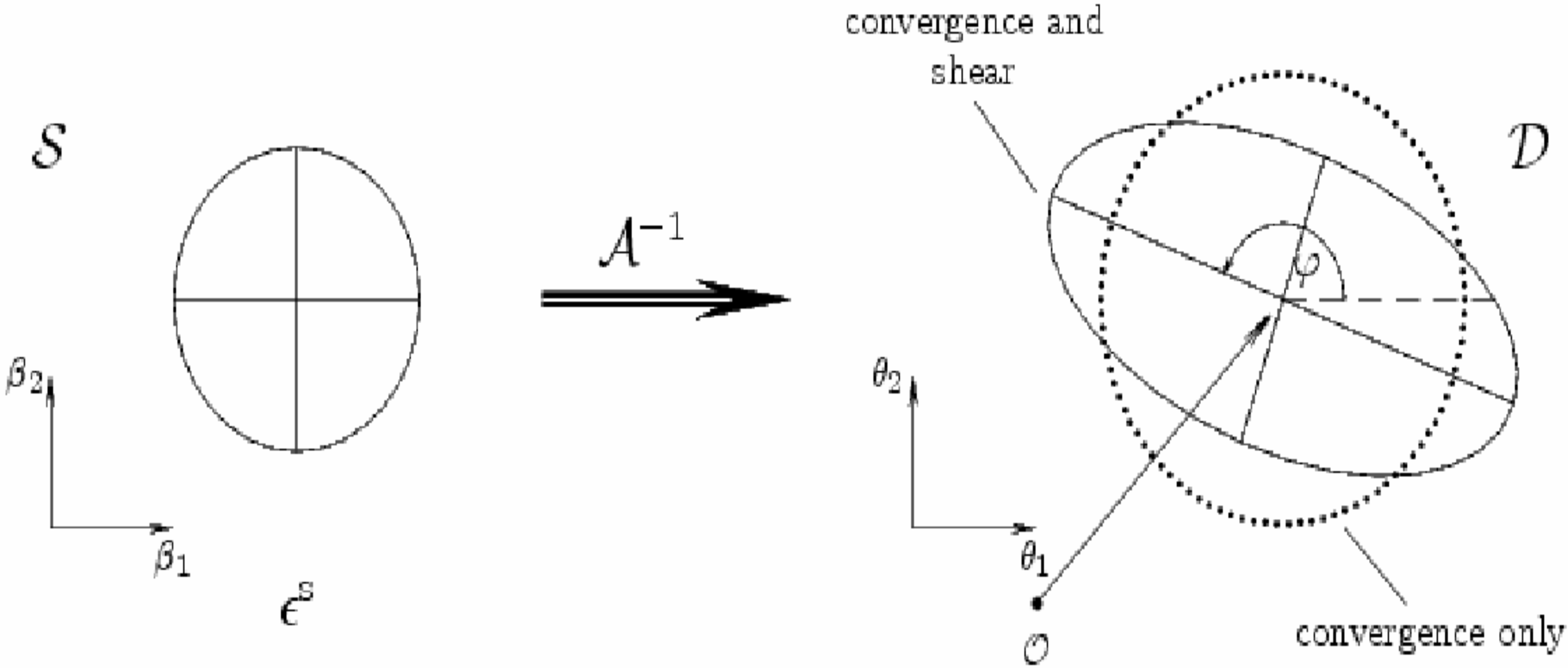

- Image and source From the magnification matrix,
  - κ expresses an isotropic magnification. It transforms a circle into a larger/smaller circle.
  - γ is an anisotropic magnification. It transforms a circle into an ellipse with minor and major axes :

$$b = (1 - \kappa + \gamma)^{-1} \ , \ a = (1 - \kappa - \gamma)^{-1}$$

Definitions of Ellipticity

$$\varepsilon = \frac{1-\frac{b}{a}}{1+\frac{b}{a}}\, e^{2i\phi} \; ; \; \chi = \frac{1-\left(\frac{b}{a}\right)^2}{1+\left(\frac{b}{a}\right)^2}\, e^{2i\phi}$$

$$\varepsilon = \frac{\chi}{1+\left(1-|\chi|^2\right)^{1/2}}$$

where

$$a = (1-\kappa-\gamma)^{-1} \text{ and } b = (1-\kappa+\gamma)^{-1}$$

ε is directly the reduced shear

$$|g| = |\varepsilon| = \frac{|\gamma|}{1-\kappa}$$

- Weak Lensing regime : $\kappa << 1,\; |\gamma| << 1 \; |g|^2 \simeq 0$ Therefore

$$\boxed{g = \frac{\gamma}{1-\kappa} \simeq \gamma}$$

$$\chi \simeq \chi^S + 2\left(g - \chi^S \Re\left(g\chi^*\right)\right)$$

Source orientation
Isotropically istributed

$$\langle \chi^S \rangle \simeq 0$$

->

$$\langle \chi \rangle \simeq 2\gamma = 2g$$

Image ellipticity unbaiased
estimate of shear

n

Weak lensing mass reconstruction

$$\gamma(\theta) = \frac{1}{\pi}\int \kappa(\theta') F(\theta - \theta') \, d\theta^2$$

*

$$F(\theta) = \frac{\theta_1^2 - \theta_2^2 + 2i\theta_1\theta_2}{|\theta|^4} = F_1(\theta) + iF_2(\theta)$$

In Fourier space

$$\kappa(\theta) = \frac{1}{(2\pi)^2}\int \hat{\kappa}(\mathbf{k}) e^{i\mathbf{k}.\theta} \, d^2k$$

Eq. * , convolution

$$\hat{\gamma}(\mathbf{k}) = \frac{1}{\pi}\hat{\kappa}(\mathbf{k}) \hat{F}(\hat{k})$$

Inverting

$$\kappa(\theta) = \frac{1}{\pi}\int \hat{F}^*(\theta - \theta') \gamma(\theta') \, d\theta^2 + \kappa_0$$

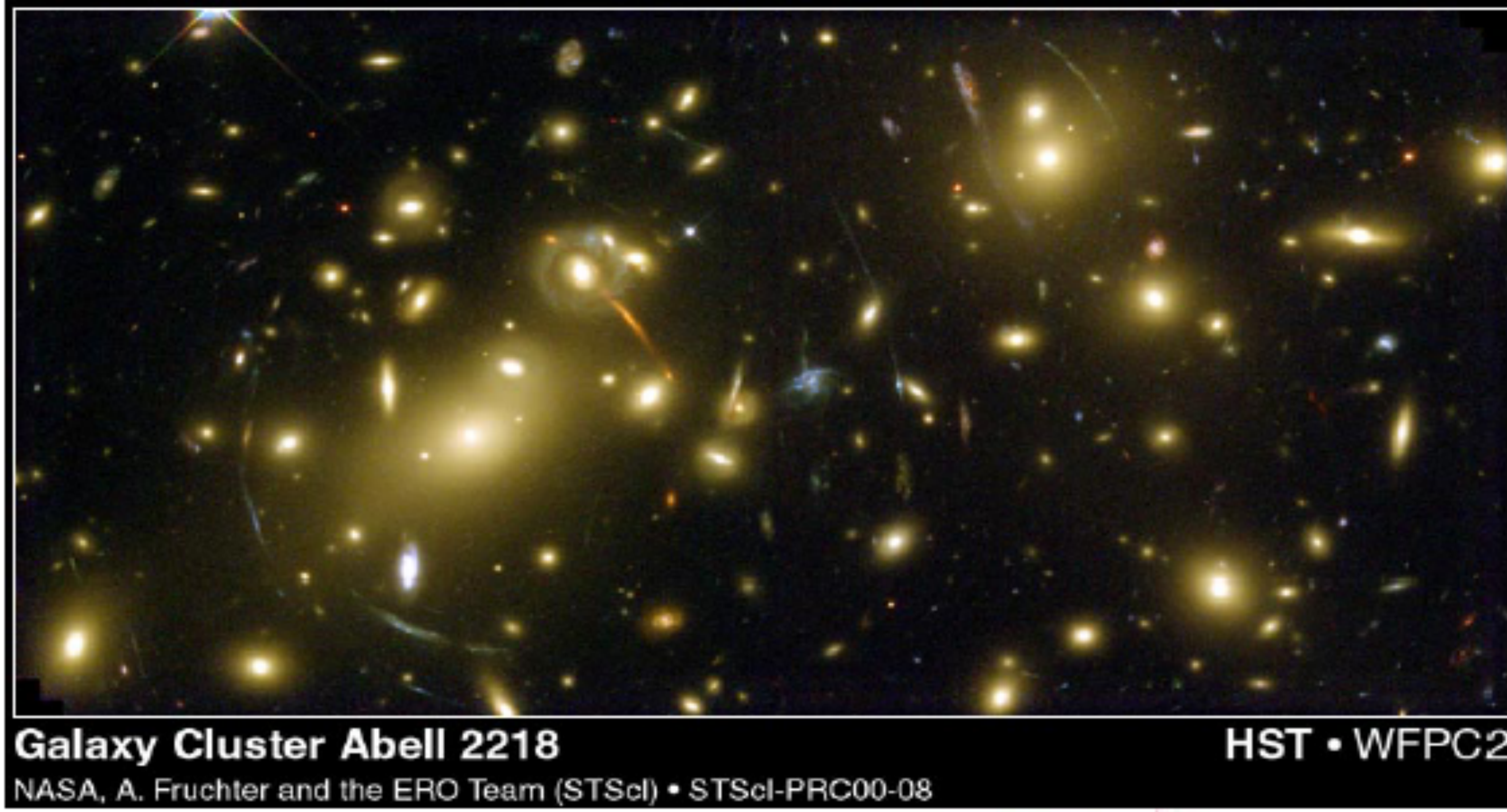

Mass reconstruction of the

Lensing cluster Abell 2218

(z=0.18)

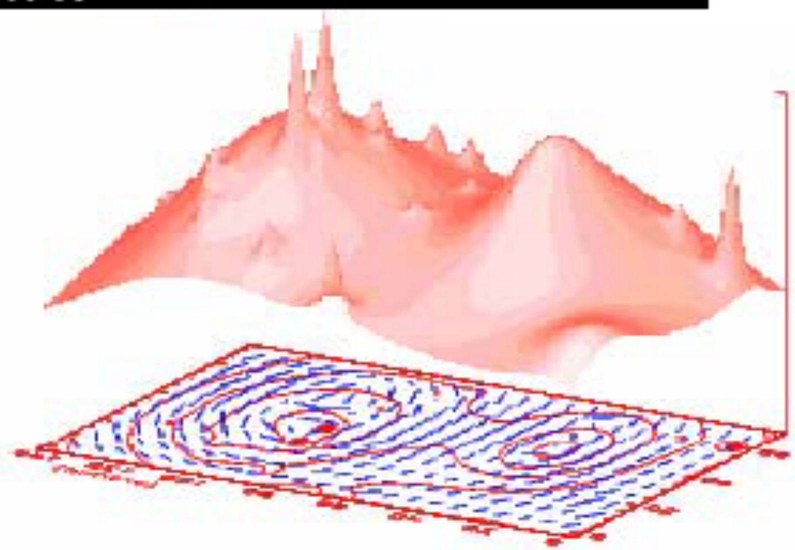

Typical values:

- For a lens of 1 solar mass located at 1 AU and a source a 1 kpc

  θ_E= 0.003 arc-second

- For a lens of 10^{11} solar masses located at 100kpc and a source at 300 kpc

  θ_E= 1 arc-second

- For a lens of 10^{15} solar masses located at 1Gpc and a source at 3 Gpc

  θ_E= 30 arc-second (sensitive to cosmological parameters)

- Typical value: cluster of galaxies of 10^{15} solar masses at 1Gpc and sources at 2 Gpc :

$$\Sigma_{\mathrm{crit}} = 0.5 \text{ g/cm}^2$$

Comparison: typical mass density of a 1Mpc diameter cluster, based on its galaxy light distribution:

$$\Sigma_{\text{,,light''}} = 0.02 \text{ g/cm}^2$$

lass profiles from weak lensing

Lensing equation for the observed tangential shear

e.g. Schneider, 1996

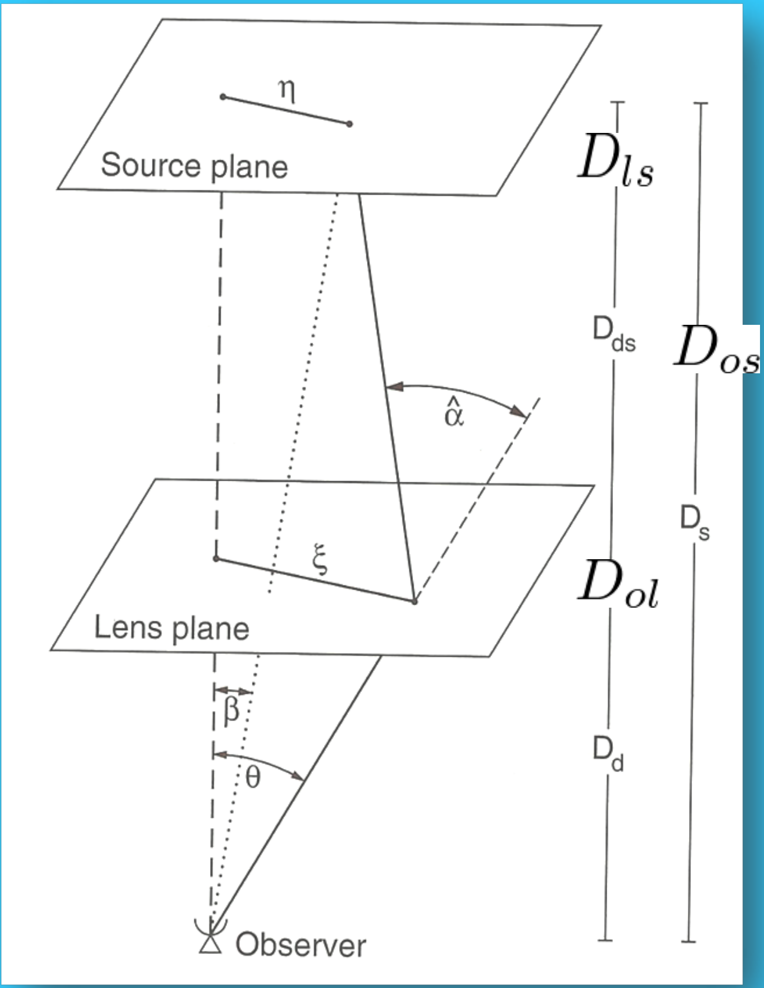

$$\gamma = \gamma_t + i\gamma_\times$$

Shear= Tangential term+curl

For a circularly symmetric lens the curl vanish and the tangential part is

$\gamma \rightarrow \gamma_t$

$$\langle \gamma_t \rangle \equiv \frac{\bar{\Sigma}(R) - \Sigma(R)}{\Sigma_c(R)}$$

$$\Sigma_c = \frac{c^2}{4\pi G} \frac{D_{os}}{D_{ol} D_{ls}}$$

$$\Sigma(R) = 2\int_0^\infty \rho(R,z)\,dz$$

Projected mass density of the object distorting the galaxy

$$\bar{\Sigma}(R) = \frac{2}{R^2}\int_0^R x\Sigma(x)\,dx$$

Mean projected mass density interior to the radius R

$$\bar{\Sigma} = \frac{M(R)}{4\pi R^2}$$

$$R = \theta D_{ol}$$

The DM distribution is obtained by fitting the observed shear with a chosen density profile with 2 free parameters.

MODELLING WEAK LENSING SIGNALS (galaxies)

Lenses: 170 000 isolated galaxies, sources: 3 10^7 SDSS galaxies

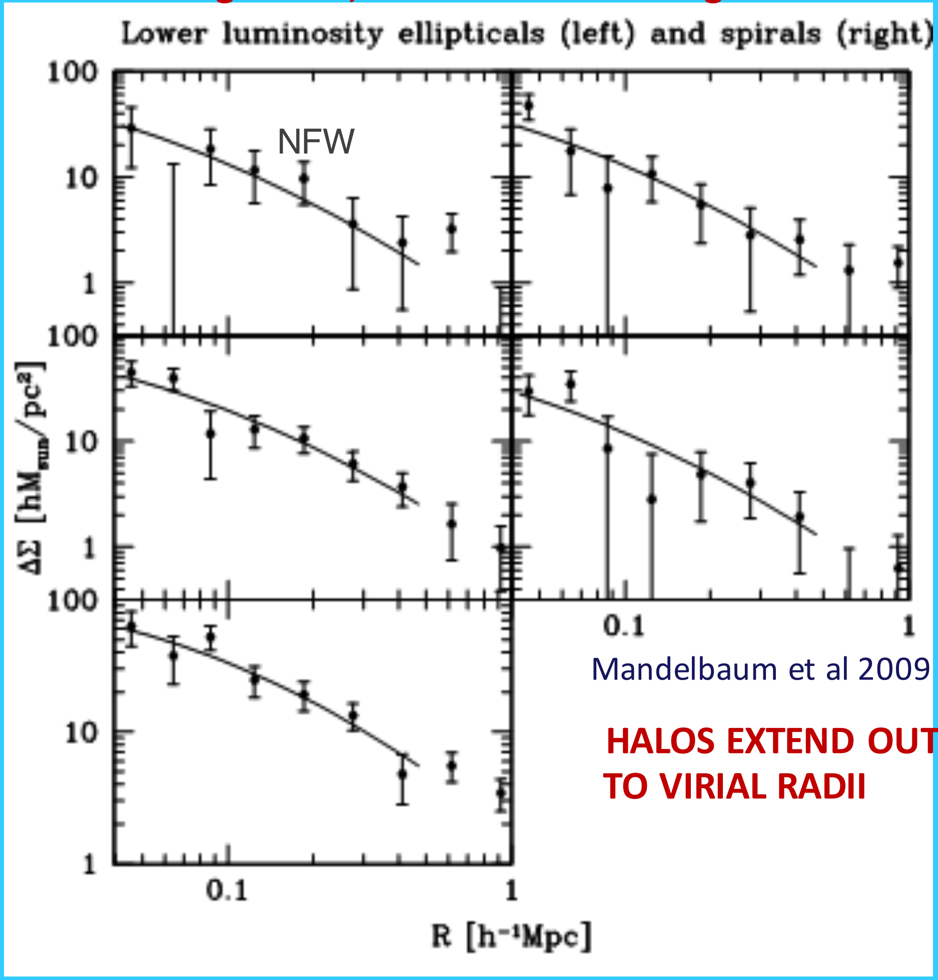

Using the previous method, Mandelbaum et al. (2006, 2009) measured the shear around galaxies of different luminosities out to 500 - 1000 kpc reaching out the virial radius, although with a not negligible observational uncertainty. Both NFW and Burkert halo profiles agree with data.

OUTER DM HALOS: NFW/BURKERT PROFILE FIT THEM EQUALLY WELL

Donato et al 2009

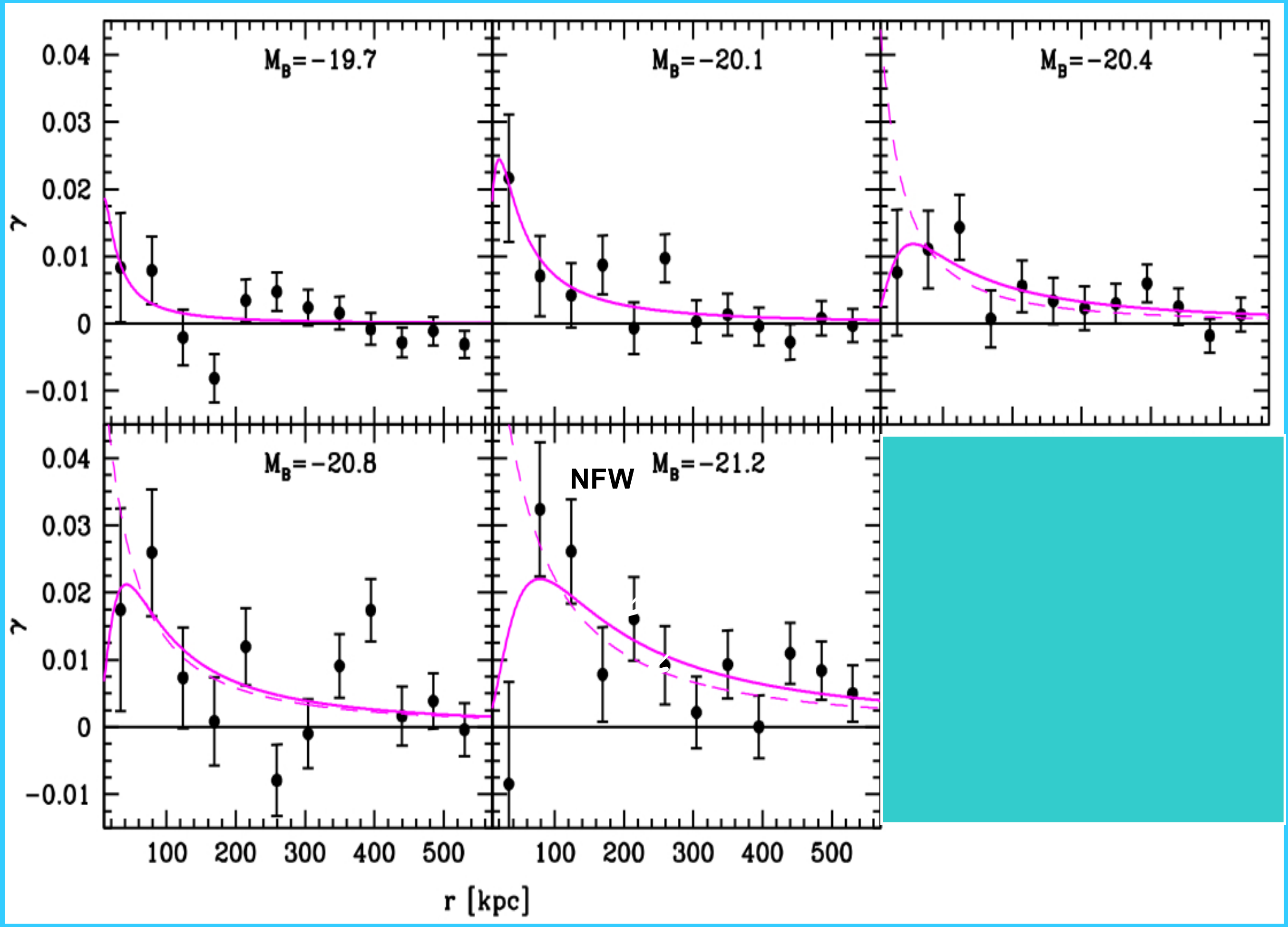

Tangential shear measurements from Hoekstra et al. (2005) as a function of projected distance from the lens in five R-band luminosity bins. In this sample, the lenses are at a mean redshift z ~ 0.32 and the background sources are, in practice, at z=∞. The solid (dashed) magenta line indicates the Burkert (NFW) model fit to the data. At low luminosities they agree.

Weak and strong lensing

strong lensing measures the total mass inside the Einstein ring

Sloan Lens ACS (SLACS):
(Gavazzi et al. 2007)

Strong lensing data of 22 massive SLACS galaxies modeled as a sum of stellar component (de Vaucoulers) + DM halo (NFW)

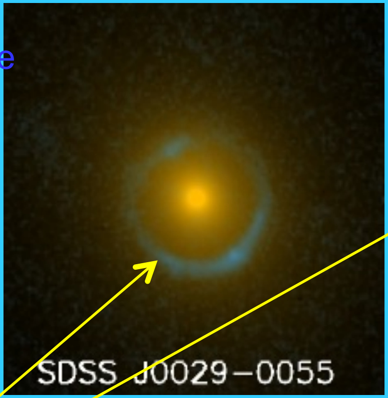

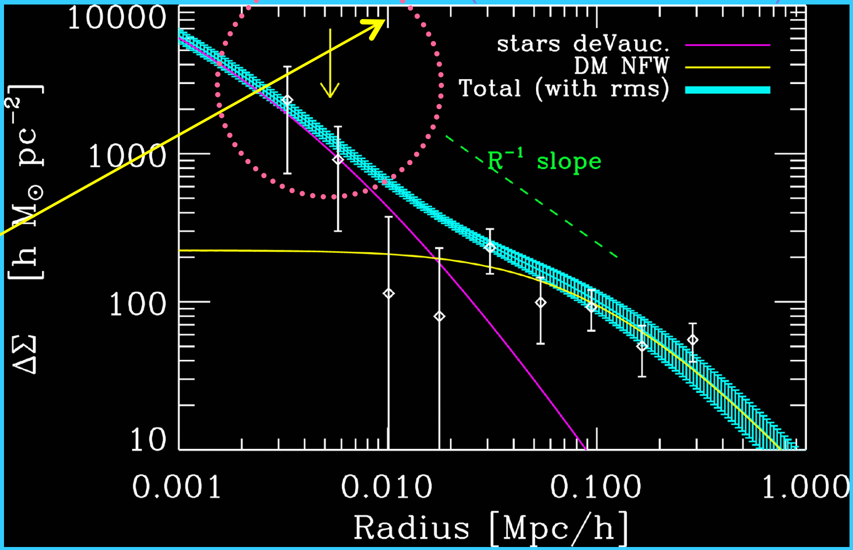

AN EINSTEIN RING AT $\mathbf{R_{einst}}$ IMPLIES THERE A CRITICAL SURFACE DENSITY:

$$\Sigma(R_{Einst}) = \frac{0.35}{D\ (Gpc)}\ g/cm^2 \qquad D = \frac{D_{os}}{D_{ol} D_{ls}}$$

Shear profile for the best DM + de Vaucouleurs profile

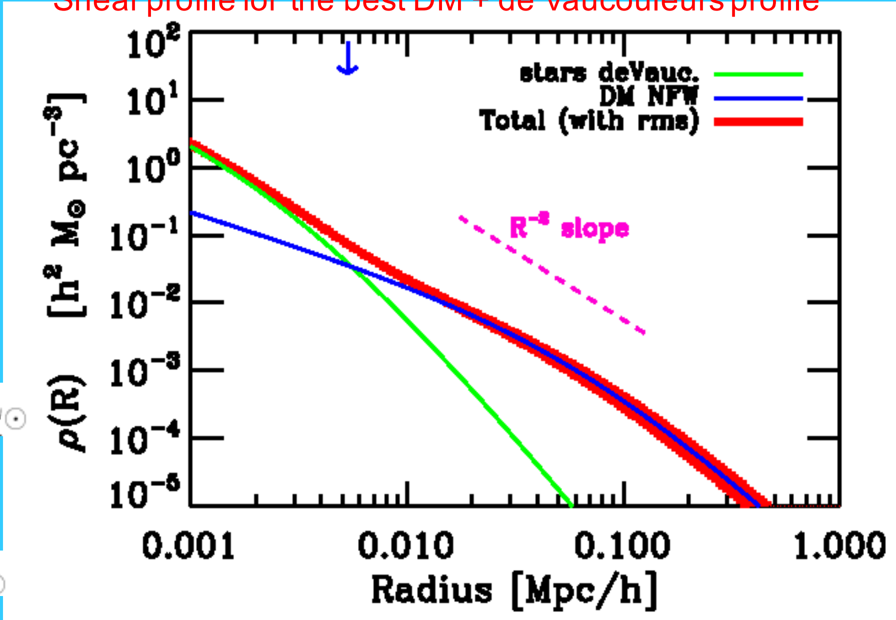

The thickness of the total mass curve codes for the 1 sigma uncertainty around the total shear profile. Uncertainties are very small below 10 kpc because of strong lensing data not shown here. The transition between star and DM-dominated mass profile occurs close to the mean effective radius (yellow arrow). The total density profile is close to isothermal over ~ 2 decades in radius..

$$\Upsilon_V = 4.48 \pm 0.46\, h M_\odot / L_\odot \qquad \Upsilon_B = 4.17 \pm 0.44\, M_\odot / L_\odot$$

M3D $200\, h^{-1}\,\mathrm{kpc}) = (8.1 \pm 1.8) \times 10^{12}\, h^{-1} M_\odot$

$$M_{2D}(< 200\, h^{-1}\,\mathrm{kpc}) = (10.8 \pm 2.7) \times 10^{12}\, h^{-1} M_\odot$$

Strong lensing and galaxy kinematics

Assume $\rho_{tot}(r) = \rho_0(r/r_0)^\gamma$ $\rho_{sph}(r) = \frac{M_{sph}}{4\pi}\frac{R_e}{r(r+R_e/1.8)^3}$ Koopmans, 2006

Fit $M_{tot}(R_{Einst}), \sigma_{ap}(R)$

γ= logarithmic slope

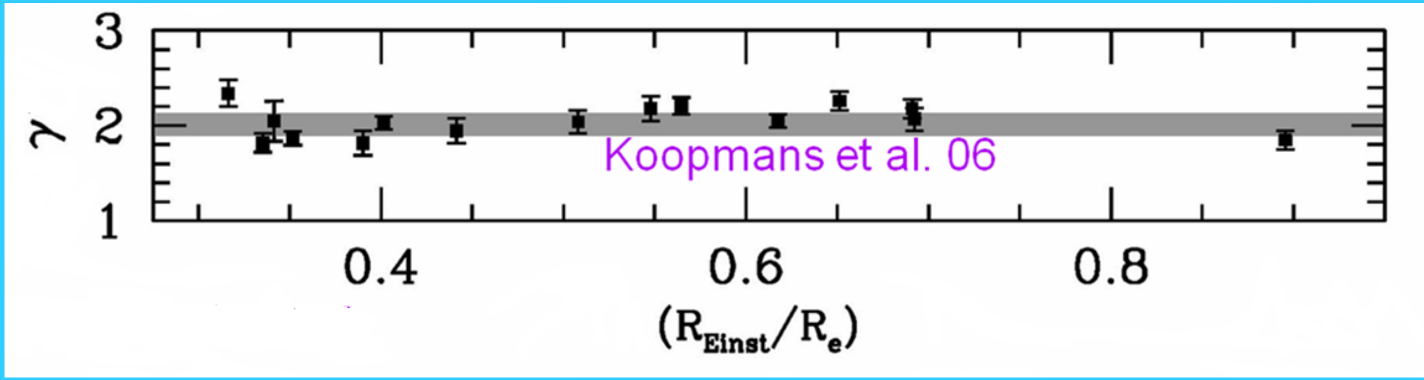

Koopmans et al. (2006): joint gravitational lensing and stellar-dynamical analysis of a subsample of 15 massive field early-type galaxies from SLACS Survey. Galaxies have remarkably homogeneous inner mass density profiles ($\rho_{tot} \propto r^{-2}$). Stellar Spheroid mass accounts for most of the total mass inside Re. The figure shows the logarithmic density slope of Slacs lens galaxies as a function of (normalized) Einstein radius.

- **Inside R_{Einst} the total (spheroid + dark halo) mass increase proportionally with radius**

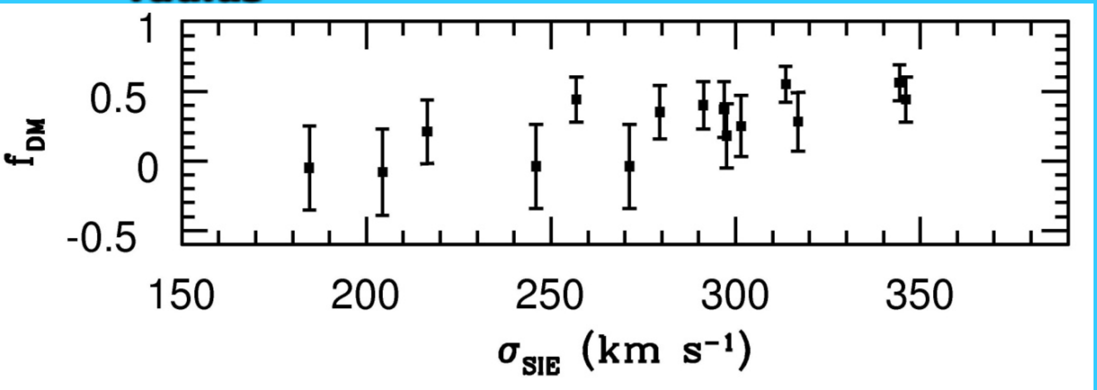

Inferred dark matter mass fraction inside the Einstein radius, assuming a constant stellar M/LB as a function of E/S0 velocity dispersion

SIE: Singular Isothermal Ellipsoid model

- **Inside R_{Einst} the total the fraction of dark matter is small**

Observational controversy: strong gravitational lensing

CL0024+1654

HST image

$Z=0.39$, $L_X=5\times10^{43}\,h^{-2}$ erg/s

reconstructed mass distribution (with 512 parameters)

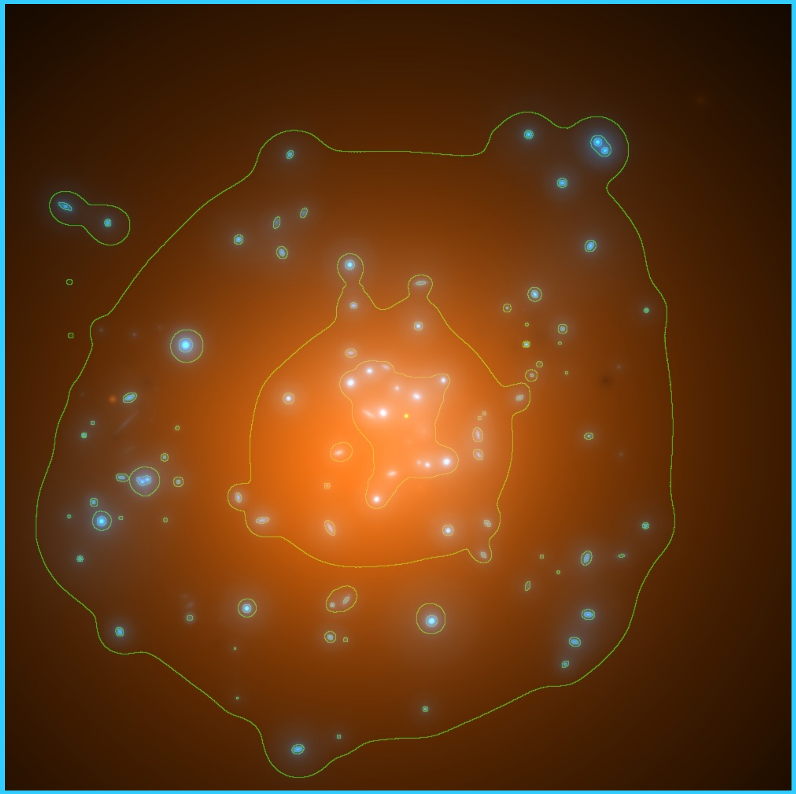

Tyson, Kochanski & Dell'Antonio (1998)

FIG. 1.—The reconstructed total mass density in CL 0024 is shown as a color-coded mass image. The DM is shown in orange. The mass associated with visible galaxies is shown in blue. The contours are at 0.5, 1, and 1.5 times the critical lensing density ($4497\,h\,d_{0.57}^{-1}\,M_\odot\,\mathrm{pc}^{-2}$), with heavier contour at the critical lensing density. This image is 336 h^{-1} kpc across. North is up, and east is left.

*

CL0024+1654

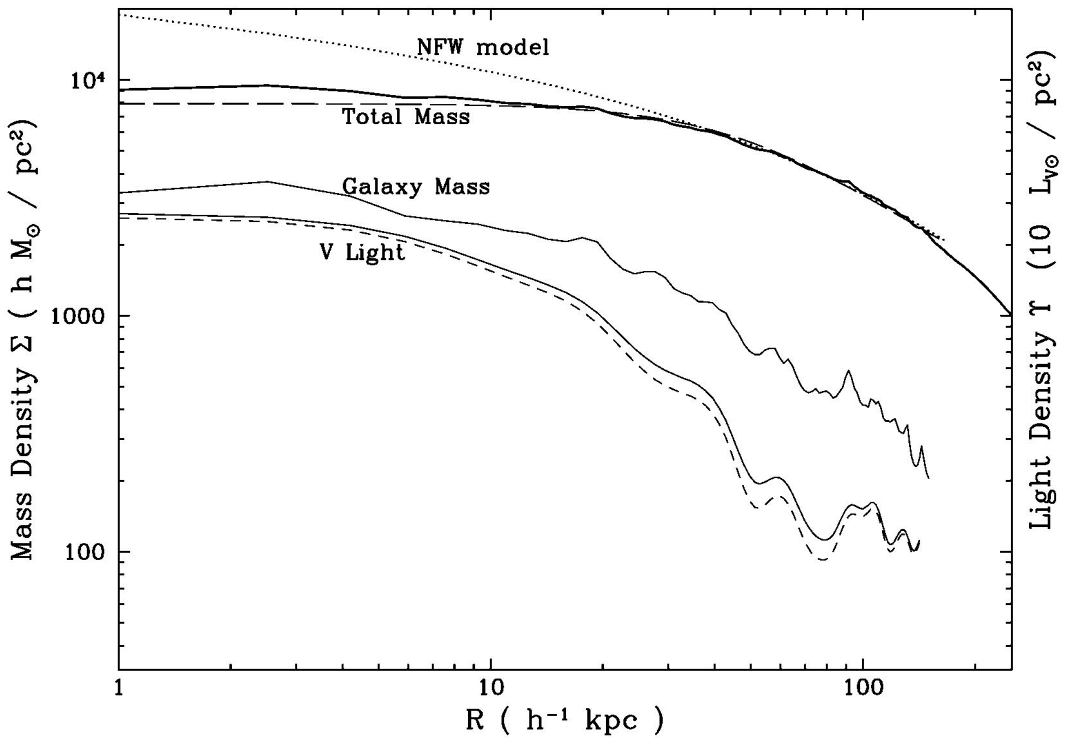

FIG. 4.—A radial plot of the mass density and light density. Total (*thick line*) and galaxy-only (*thin line*) components of the mass are shown. The dotted line is the best NFW fit discussed in the text, and the dashed line is the best-fit single PL model. The 35 h^{-1} kpc soft core in the mass is evident. A singular mass distribution is ruled out. The total rest-frame V light profile (*solid line*) and galaxy V light profile (*dashed line*), smoothed with a 5 h^{-1} kpc Gaussian, are also shown.

InnerSlope= 0.57 ± 0.02

Tyson, Kochanski & Dell'Antonio (1998)

*

- Gavazzi et al 2003 analyzed the radial mass profile of MS2137.3-2353 (rich cD cluster at z=0.313) and found that:

1. Observations seems to favor isothermal profiles with flat core or generalized-NFW profiles with $0.8 \leq \alpha \leq 1.2$ without introducing the fifth image knowledge.
2. When this constraint is added, they favor a flat core softened isothermal spheres.
3. Isothermal sphere fits the system better than generalized NFW (where inner slope is allowed to vary).

How to decide the mass profile using gravitational lensing ?
One usually model the system using some profiles (such as isothermal sphere or NFW) and then try to generate arcs that matches what are observed.

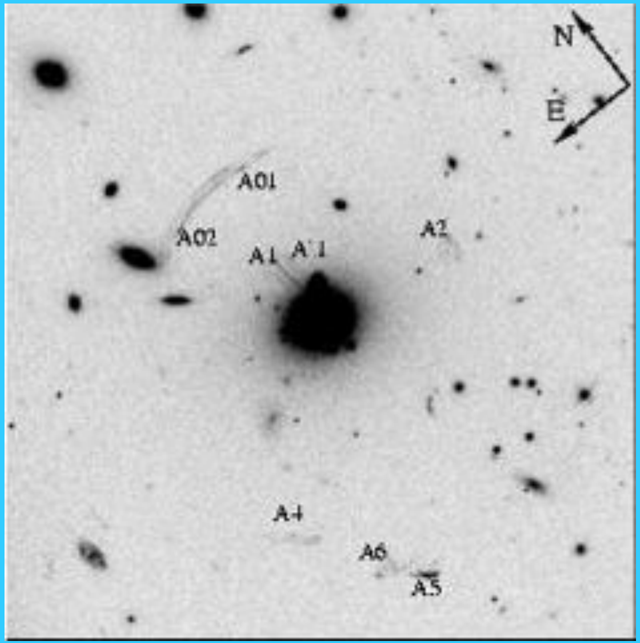

Gavazzi et al. 2003

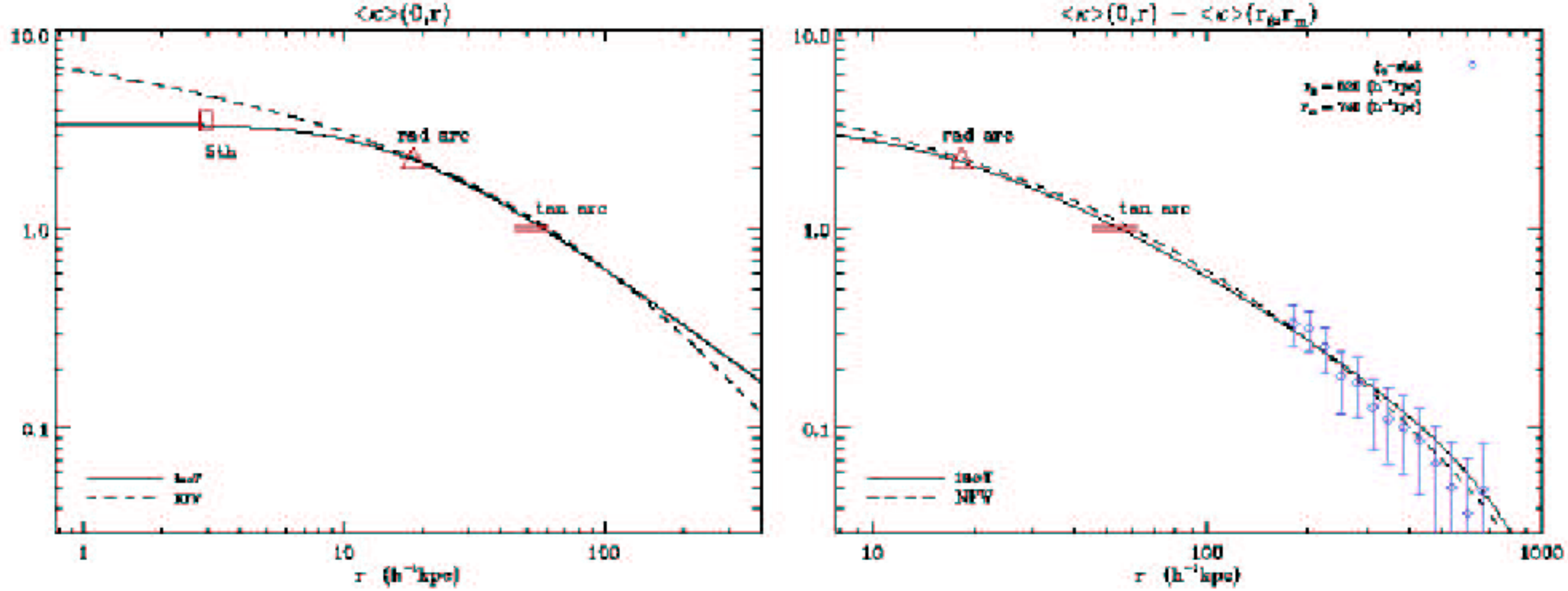

Fig. 5. Projected mean surface density. Solid: NFW best fit, dashed: IS. Notice how models match near the arcs locations. Between 2.5 and 28 arc-sec, the mean convergences $\bar{\kappa} = <\kappa> (0, r)$ differ from each other by less than 3 percents. Faint discrepancies appear in the outer regions through weak lensing signal and at the very center. Constraints due to the fifth image candidate are detailed in Sect. 3.4.3. The weak lensing data are deduced from the ζ_c-statistic.

*

Observational controversy: clusters

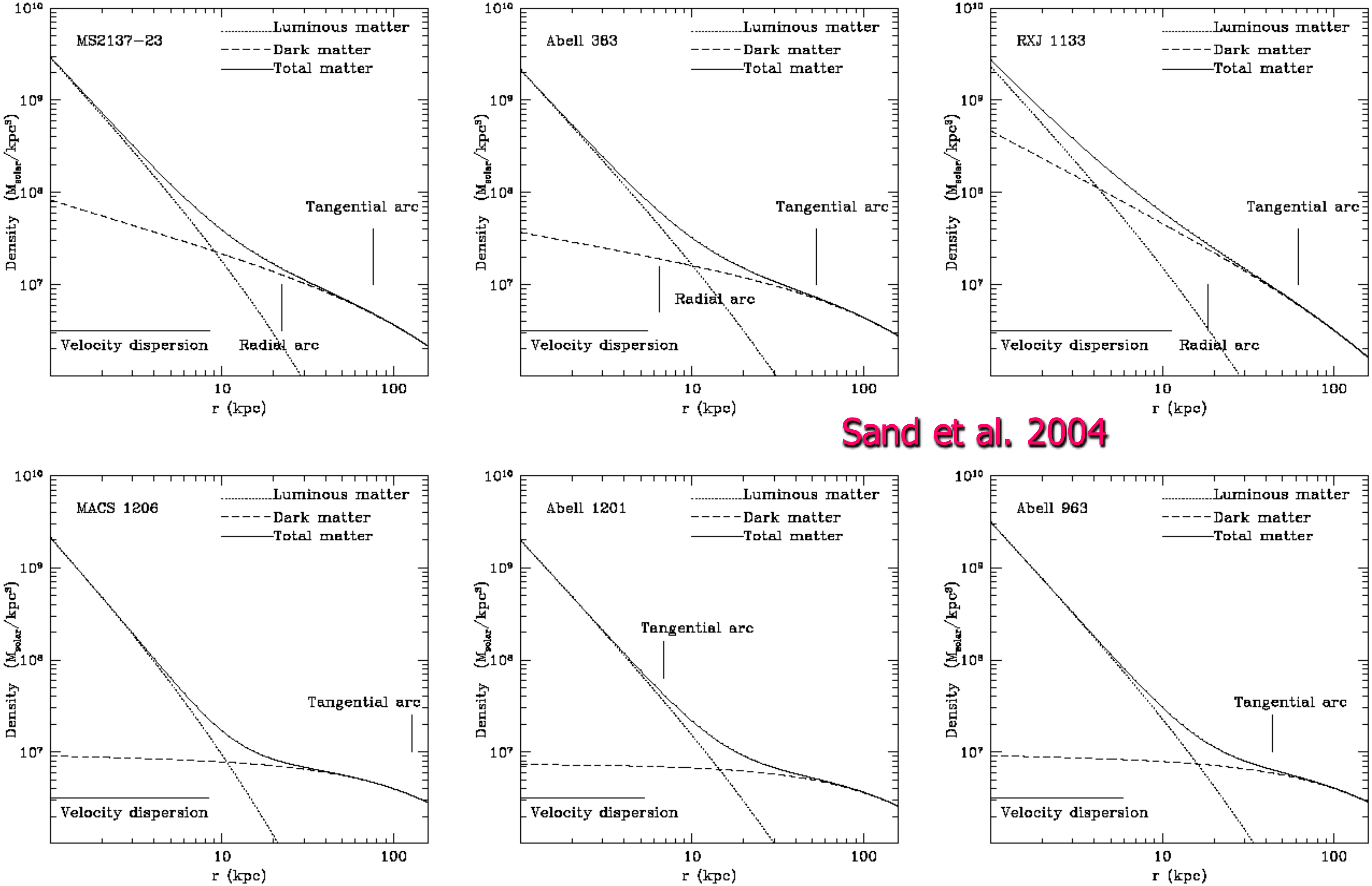

Sand et al. 2004

FIG. 8.—Best-fitting total density profile for the entire sample. The positions of the gravitational arcs and the range over which we were able to measure the velocity dispersion profile are noted. Within ≲10 kpc the total density distribution is dominated by the BCG.

*

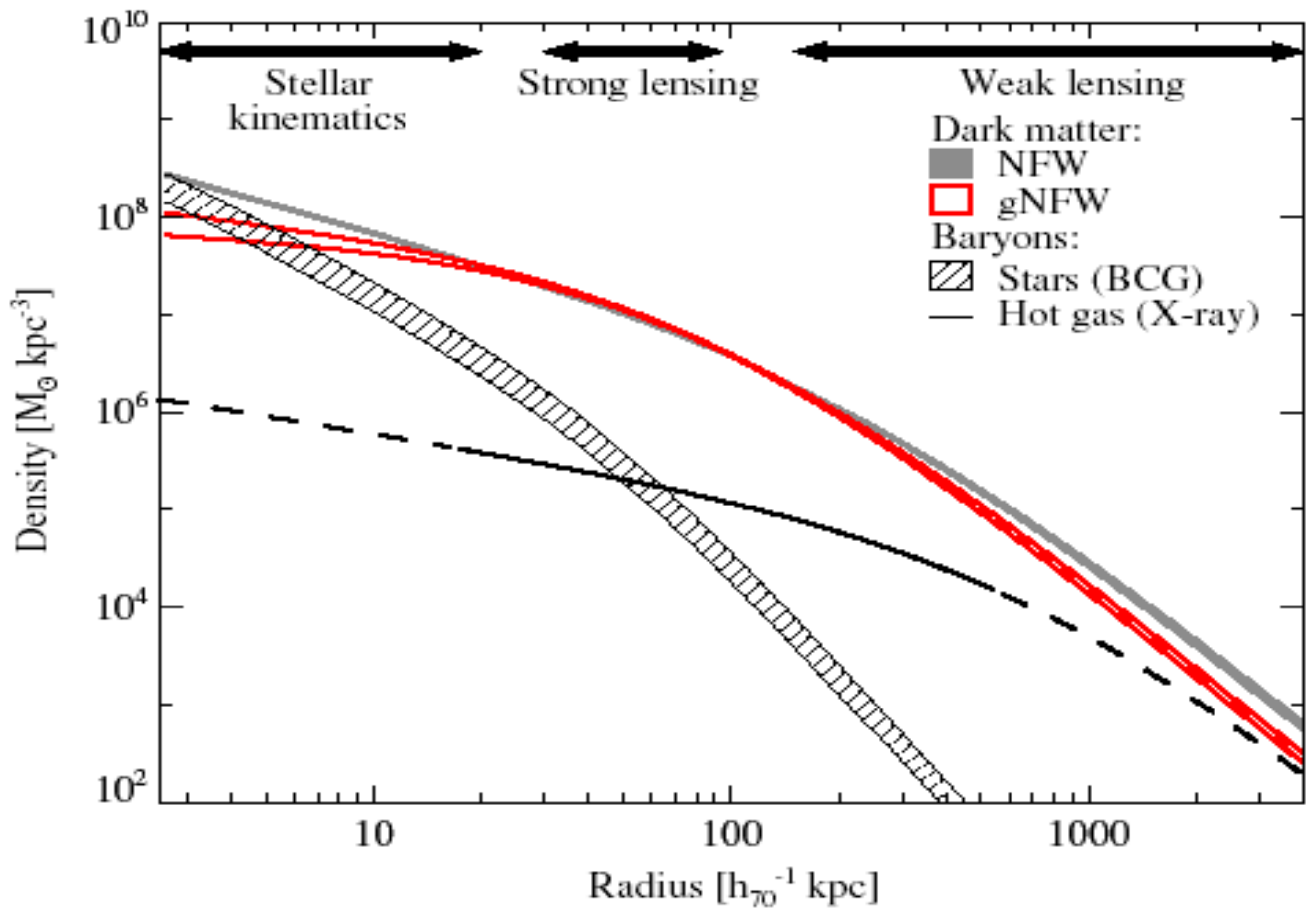

density profiles inferred from (g) NFW fits to the combined data set. The BCG profile is also shown, using the M_*/L ratios inferred in the gNFW model, along with the X-ray gas profile provided by S. Allen (Section 5.3). For reference, the dashed line gives a gNFW extrapolation of the hot gas outside the range of the X-ray data.

A611
Newmann
et al. (2009)

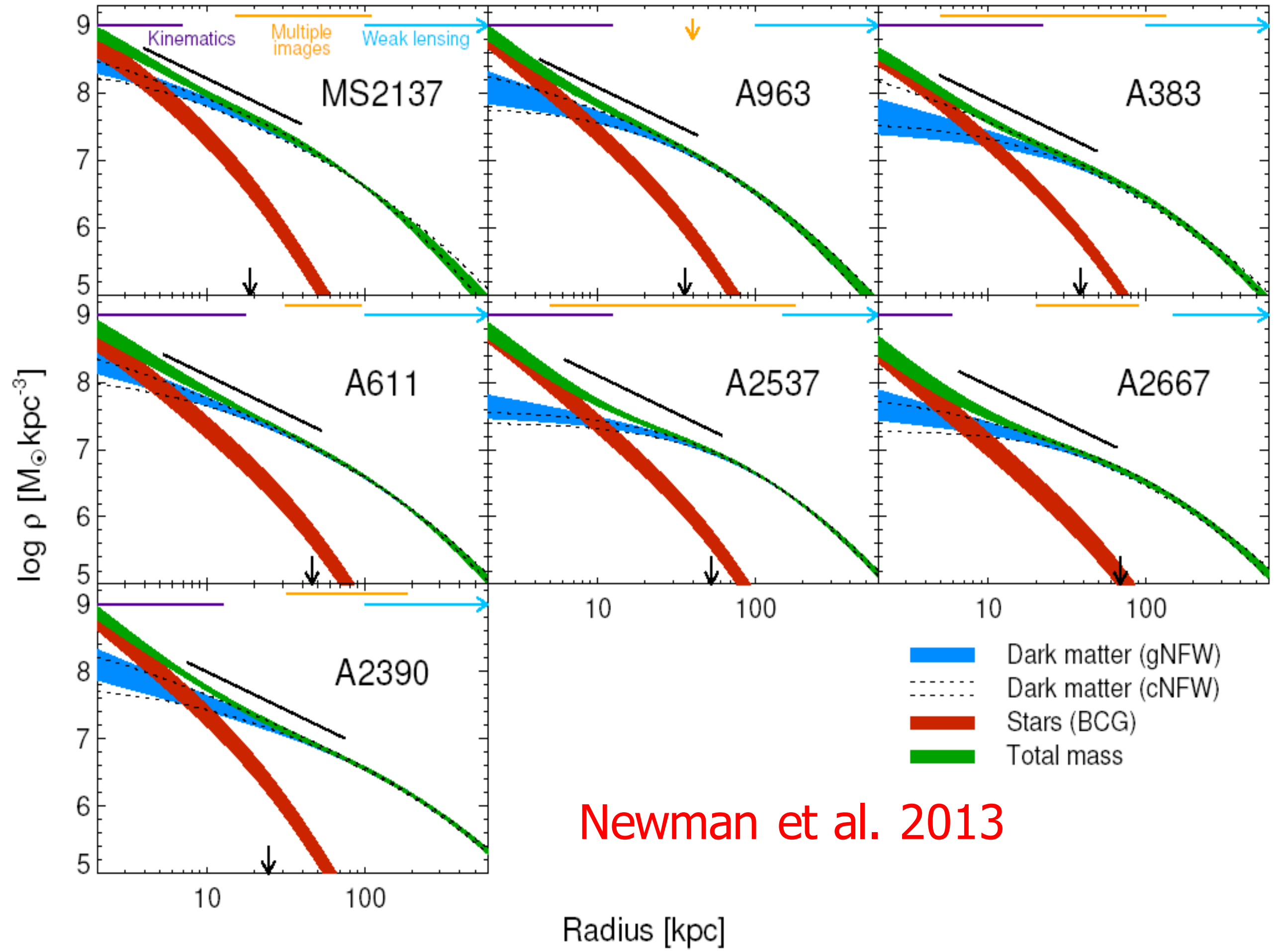

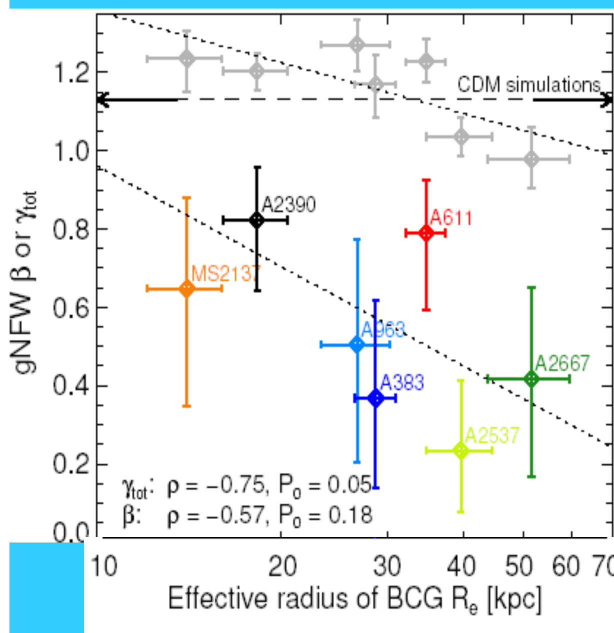

FIG. 3.— Radial density profiles for the DM halo, stars in the BCG, and their total in each cluster, adopting the joint constraint on $\log \alpha_{\rm IMF}$ from Figure 2. The spatial extent of each data set is indicated at the top of each panel. The black line segment spans $r/r_{200} = 0.003 - 0.03$ and has the slope $\rho \propto r^{-1.13}$ that is the average of clusters in the Phoenix DM-only simulations (Gao et al. 2012b) over the same interval (Paper I, Section 10). The width of the bands indicates the uncertainty, including both 1σ random uncertainties for isotropic models and a systematic component estimated by taking $\beta_{\rm aniso} = \pm 0.2$ (Section 4.3). Arrows at the bottom of each panel indicate three-dimensional half-light radius r_h of the BCG.

THE SURPRISINGLY STEEP MASS PROFILE OF ABELL 1689, FROM A LENSING ANALYSIS OF SUBARU IMAGES[1]

TOM BROADHURST[2], MASAHIRO TAKADA[3], KEIICHI UMETSU[4], XU KONG[5], NOBUO ARIMOTO[5], MASASHI CHIBA[3], TOSHIFUMI FUTAMASE[3]

Draft version June 30, 2005

ABSTRACT

Subaru observations of A1689 ($z = 0.183$) are used to derive an accurate, model-independent mass profile for the entire cluster, $r \lesssim 2\mathrm{Mpc}/h$, by combining magnification bias and distortion measurements. The projected mass profile steepens quickly with increasing radius, falling away to zero at $r \sim 1.0\mathrm{Mpc}/h$, well short of the anticipated virial radius. Our profile accurately matches onto the inner profile, $r \lesssim 200\mathrm{kpc}/h$, derived from deep HST/ACS images. The combined ACS and Subaru information is well fitted by an NFW profile with virial mass, $(1.93 \pm 0.20) \times 10^{15} M_\odot$, and surprisingly high concentration, $c_{\mathrm{vir}} = 13.7^{+1.4}_{-1.1}$, significantly larger than theoretically expected ($c_{\mathrm{vir}} \simeq 4$), corresponding to a relatively steep overall profile. A slightly better fit is achieved with a steep power-law model, $d \log \Sigma(\theta)/d \log \theta \simeq -3$, with a core $\theta_c \simeq 1.'7$ ($r_c \simeq 210\mathrm{kpc}/h$), whereas an isothermal profile is strongly rejected. These results are based on a reliable sample of background galaxies selected to be redder than the cluster E/S0 sequence. By including the faint blue galaxy population a much smaller distortion signal is found, demonstrating that blue cluster members significantly dilute the true signal for $r \lesssim 400\mathrm{kpc}/h$. This contamination is likely to affect most weak lensing results to date.

Subject headings: cosmology: observations – gravitational lensing – galaxies: clusters: individual(Abell 1689)

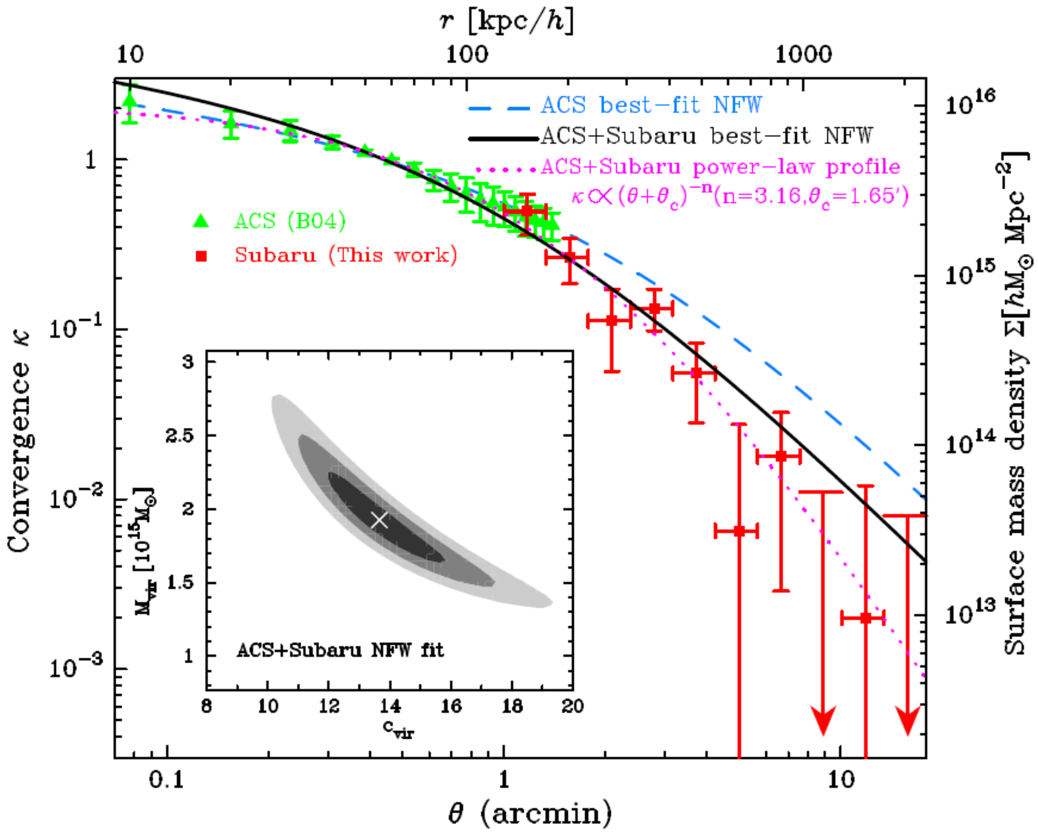

FIG. 3.— Reconstructed mass profile. The triangle and square symbols with error bars show the results from the ACS strong lensing analysis (B04) and the Subaru weak lensing analysis (this work), respectively. The dashed and solid curves show the best-fitting NFW profiles for the ACS data alone and for the combined ACS+Subaru profile, respectively. The best-fitting NFW profile for the ACS+Subaru profile has a high concentration, $c_{\mathrm{vir}} = 13.7$, and somewhat overestimates the inner slope and is a bit shallow at large radius. A cored power-law provides a better fit to the full projected mass profile. The inset plot shows the 68%, 95% and 99.7% confidence levels in the (c_{vir}, M_{vir}) plane for the ACS+Subaru NFW fitting ($\Delta\chi^2 = 2.3$, 6.17 and 11.8).

Abell 1689 (also Abell 2218): gravitational arcs near the center.

Results calibrated by strong gravitational lensing (green points in the figure).

*

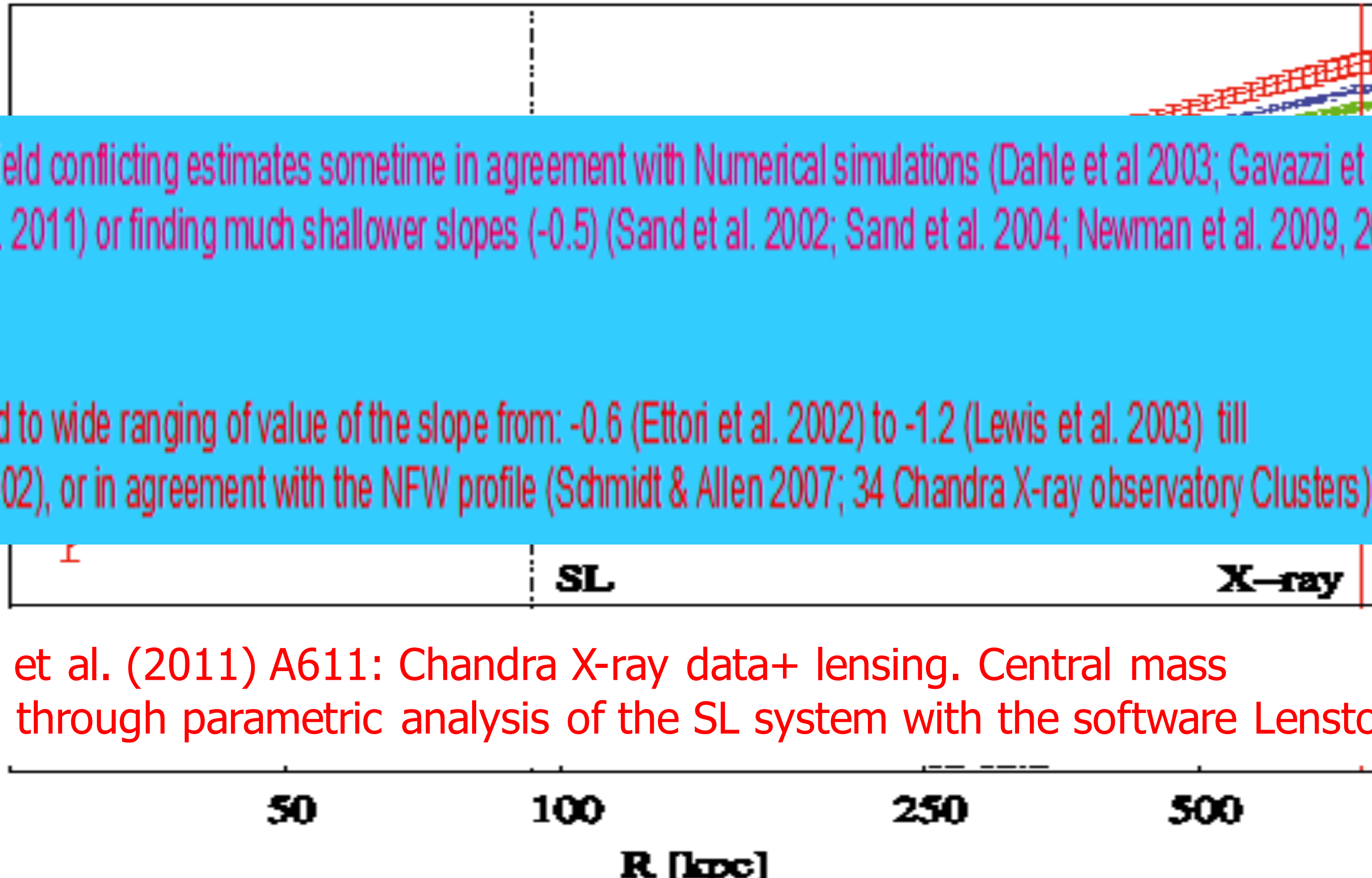

Gravitational lensing yield conflicting estimates sometime in agreement with Numerical simulations (Dahle et al 2003; Gavazzi et al. 2003; Donnaruma et al. 2011) or finding much shallower slopes (-0.5) (Sand et al. 2002; Sand et al. 2004; Newman et al. 2009, 2011, 2012)

X-ray analyses have led to wide ranging of value of the slope from: -0.6 (Ettori et al. 2002) to -1.2 (Lewis et al. 2003) till -1.9 (Arabadjis et al. 2002), or in agreement with the NFW profile (Schmidt & Allen 2007; 34 Chandra X-ray observatory Clusters)

Donnarumma et al. (2011) A611: Chandra X-ray data+ lensing. Central mass reconstructed through parametric analysis of the SL system with the software Lenstool

Projected 2D mass profiles obtained with the X-ray (red solid line) and with the strong lensing analyses when modelling the BCG as a dPIE (green dashed line) or a Sérsic halo (blue dashed line). The vertical lines mark the spatial range of the strong lensing (black dotted line) and X-ray (red solid line) constraints. The X-ray (strong lensing) profile was derived by measuring the enclosed mass in cylinders centred on the X-ray emission centroid [BCG].

As a comparison, we report the estimates of the projected total mass within 250 kpc obtained by Richard et al. (2010) through a strong lensing analysis (label SL-R09, marked with a filled black circle) and through an X-ray analysis by Sanderson et al. (2009a) (label X-ray-S09, marked with a filled orange square).

*

Summary

- Numerical simulations for collisionless dark matter consistently suggest the formation of a central cusp rather than a core.
- The density profile is not universal.
- Spirals: galactic rotation curves indicate a relatively flat core rather than a cusp, but gravitational lensing, in some cases, indicates the contrary.
- Ellipticals: difficulty in establishing the inner density profile shape
- dSphs: contraddicting results
- Clusters: Recent observations show cored profiles in some of them